JBC RESEARCH ARTICLE

Activity-based protein profiling reveals active serine proteases that drive malignancy of human ovarian clear cell carcinoma

Received for publication, December 15, 2021, and in revised form, June 10, 2022 Published, Papers in Press, June 16, 2022,
https://doi.org/10.1016/j.jbc.2022.102146

Christine Mehner[1,2], Alexandra Hockla[2], Mathew Coban[2], Benjamin Madden[3], Rosendo Estrada[4], Derek C. Radisky[2], and Evette S. Radisky[2,*]

From the [1]Mayo Clinic Graduate School of Biomedical Sciences, Mayo Clinic, Rochester, Minnesota, USA; [2]Department of Cancer Biology, Mayo Clinic, Jacksonville, Florida, USA; [3]Medical Genome Facility Proteomics Core, Mayo Clinic, Rochester, Minnesota, USA; [4]Peptides International, Louisville, Kentucky, USA

Edited by George DeMartino

Ovarian clear cell carcinoma (OCCC) is an understudied poor prognosis subtype of ovarian cancer lacking in effective targeted therapies. Efforts to define molecular drivers of OCCC malignancy may lead to new therapeutic targets and approaches. Among potential targets are secreted proteases, enzymes which in many cancers serve as key drivers of malignant progression. Here, we found that inhibitors of trypsin-like serine proteases suppressed malignant phenotypes of OCCC cell lines. To identify the proteases responsible for malignancy in OCCC, we employed activity-based protein profiling to directly analyze enzyme activity. We developed an activity-based probe featuring an arginine diphenylphosphonate warhead to detect active serine proteases of trypsin-like specificity and a biotin handle to facilitate affinity purification of labeled proteases. Using this probe, we identified active trypsin-like serine proteases within the complex proteomes secreted by OCCC cell lines, including two proteases in common, tissue plasminogen activator and urokinase-type plasminogen activator. Further interrogation of these proteases showed that both were involved in cancer cell invasion and proliferation of OCCC cells and were also detected in *in vivo* models of OCCC. We conclude the detection of tissue plasminogen activator and urokinase-type plasminogen activator as catalytically active proteases and significant drivers of the malignant phenotype may point to these enzymes as targets for new therapeutic strategies in OCCC. Our activity-based probe and profiling methodology will also serve as a valuable tool for detection of active trypsin-like serine proteases in models of other cancers and other diseases.

Ovarian cancer is the most lethal gynecological malignancy, with an average 5-years survival rate of only ∼50% (https://seer.cancer.gov/statfacts/html/ovary.html). Ovarian clear cell carcinoma (OCCC) is a relatively little-studied histotype of ovarian cancer with particularly poor prognosis when diagnosed in advanced stages (1–3). OCCC patients currently do not receive treatments targeted for this particular histotype but instead receive standard platinum/taxane chemotherapy, despite showing very poor response rate (1–3). The low response rate to therapy is most likely linked to genetic and phenotypic features that vary considerably among different histological subtypes of ovarian cancer (1–3). To significantly improve ovarian cancer treatment, there is urgent need to better define the underlying biology of different histotypes and their distinct paths of progression and to identify individualized therapeutic approaches based on molecular cancer drivers.

Over 700 proteases are found in the human proteome (MEROPS Peptidase Database (4)), many of which have been linked to pathological roles in cancer (5). Serine proteases of the S1 or chymotrypsin family represent the largest family (Table S1); a majority of these proteases (79 in humans) possess trypsin-like specificity for cleavage after arginine or lysine residues within peptides and proteins (Table S2). Most of these proteases are secreted, with a lesser number tethered to the extracellular cell surface (Tables S1 and S3); in general, these enzymes perform their functions extracellularly. Trypsin-like serine proteases have been identified as potent regulators of numerous pathways in humans and are vital for digestion, blood coagulation, fibrinolysis, reproduction, and immune responses (6, 7). They have also been implicated as drivers in cancer progression (5, 8, 9).

Our preliminary studies using models of OCCC implicated one or more trypsin-like serine proteases in malignant phenotypes of this cancer subtype, posing the challenge of how to identify the relevant target(s) from among 79 candidates. The identification of these specific proteases that contribute to OCCC progression could lead to novel targeted therapeutic strategies. However, proteases often show high levels of regulatory complexity and organization into activation cascades and networks, as their activity is regulated by posttranslational proteolytic activation and by interactions with endogenous inhibitors (5, 10, 11). Importantly, transcriptional profiling methods and even most proteomic profiling methods are

* For correspondence: Evette S. Radisky, radisky.evette@mayo.edu.
Present address for Christine Mehner: Department of Physiology and Biomedical Engineering, Mayo Clinic, Jacksonville, Florida, USA.

unable to discriminate among active and inactive forms and thus do not accurately reflect protease activity in complex biological samples, presenting a significant technical challenge.

Activity-based protein profiling (ABPP) is a method of proteomic profiling in which activity-based molecular probes are employed to identify and quantify enzymes on the basis of enzyme activity rather than simple protein abundance. When applied to identification of proteases, an advantage is the ability to distinguish the population of active proteases of a particular family, unconfounded by inactive zymogen forms or inhibited proteases (10, 12, 13). Furthermore, some activity-based probes can be reliably used within living systems (10, 12, 13). Activity-based probes are generally designed to bind specifically in the active site of an enzyme or class of enzymes and to react irreversibly with catalytic residues in the enzyme active site, *via* a reactive "warhead". The warhead is connected *via* a peptide or chemical linker to an isotope, fluorescent, and/or affinity tag utilized for detection and/or purification of the probe-labeled protein population (12). The target enzyme class dictates the choice of electrophile; for example, global detection of serine hydrolases can be achieved through fluorophosphonate electrophiles, which are highly reactive to capture this diverse pool of enzymes (14, 15). To target proteases specifically, less broadly reactive electrophiles have been developed; warheads that have been employed to selectively target serine proteases over other serine hydrolases include peptidyl diphenylphosphonates (16–19), 4-chloro-isocoumarins (20, 21), and phosphoramidites (22). Peptidyl groups adjacent to the warhead form interactions with the substrate binding subsites of target proteases, and may further restrict selectivity of the probe to protease subsets or even to individual targets (18, 23, 24).

Here, we aimed to broadly profile active serine proteases with trypsin-like specificity, to identify those that drive malignancy in OCCC. Whereas previously developed probes of trypsin-like enzymes featured lysine diphenylphosphonate warheads as substrate mimics (19, 25, 26), here we aimed to achieve more comprehensive coverage of the pool of potential targets by employing an arginine diphenylphosphonate warhead, since >80% of human trypsin-like proteases show preference for Arg over Lys at the P_1 subsite[†], whereas only one (1.5%) shows marked preference for Lys over Arg (see Tables S1 and S2). Not finding the desired features among commercially available reagents, we developed a novel probe for our purpose. Additional features of our probe include an extended generic protease recognition sequence spanning P_4 – P_1 subsites, a biotin handle to facilitate affinity purification of labeled proteases, and an intervening tobacco etch virus (TEV) protease cleavage site for compatibility with tandem orthogonal proteolysis-ABPP approaches (27, 28). The rationale for inclusion of the TEV protease site is to enable selective proteolytic release of probe-labeled proteins or peptides captured on streptavidin beads for proteomic analysis, thus eliminating background from proteins that bind nonspecifically.

The probe, which showed high stability in aqueous cell culture medium, was used to profile the secreted proteome of two cultured OCCC-derived cell lines. We identified multiple active serine proteases in each OCCC cell line, including two proteases in common, tissue plasminogen activator (tPA) and urokinase-type plasminogen activator (uPA). We interrogated the involvement of these proteases in malignant phenotypes of the OCCC cell lines and found both proteases to be involved in cancer cell invasion and proliferation. Thus, our activity-based probe of trypsin-like serine proteases successfully identified two mediators of tumor progression in OCCC, which may offer targets for new therapeutic strategies. Our probe and approach also offer valuable tools for detection of active trypsin-like serine proteases in models of other cancers and other diseases.

Results

Trypsin inhibitors implicate unknown active trypsin-like serine proteases as drivers of OCCC invasion and proliferation

A sensitivity screen of cancer cell lines toward diminazene aceturate (Fig. 1*A*), a drug which we and others have previously identified as an inhibitor of trypsin-like serine proteases (29–31), showed significant inhibition of malignant phenotypes of multiple OCCC cell lines. In JHOC5 and JHOC9 cell lines, representative models of OCCC, we detected significant sensitivity as exemplified by phenotypic assays for both invasion (Fig. 1, *B* and *C*) and proliferation (Fig. 1, *D* and *E*), suggesting that targets of diminazene are important drivers of OCCC malignancy.

Because diminazene is also an activator of angiotensin-converting enzyme 2 (32) and may potentially exert effects on cells *via* this or other alternative targets, we sought to corroborate our initial findings using additional broad-spectrum trypsin inhibitors gabexate mesylate (Fig. S1*A*) (33) and hydroxystilbamidine (Fig. S2*A*) (31). Consistent with the effects of diminazene, gabexate mesylate and hydroxystilbamidine both similarly inhibited the invasion and proliferation of OCCC cell lines JHOC5 and JHOC9 (Figs. S1, *B–E* and S2, *B–E*). Given that the three compounds possess different chemical scaffolds and are not reported to inhibit any nonprotease targets in common, we interpret our observations as evidence of involvement of trypsin-like serine proteases in the invasion and proliferation of OCCC.

To identify the specific targets that are key to these phenotypic changes, we initially evaluated expression of the three human trypsin isoforms, each of which has been described previously among potential malignant drivers in other types of ovarian cancer (34–36) and each of which is inhibited by diminazene with low micromolar affinity (31). However, in the OCCC cell lines, we found trypsins to be either undetected or barely expressed at levels below that of normal ovarian surface epithelium cells (Fig. S3). Thus, we

[†] Substrate residues surrounding the cleavage site are numbered P_1, P_2, P_3, etc. in the direction of the N-terminus and P_1', P_2', P_3', etc. in the direction of the C-terminus, following the nomenclature of Schechter and Berger (87). The identity of the P_1 residue is a primary determinant of substrate specificity for serine proteases.

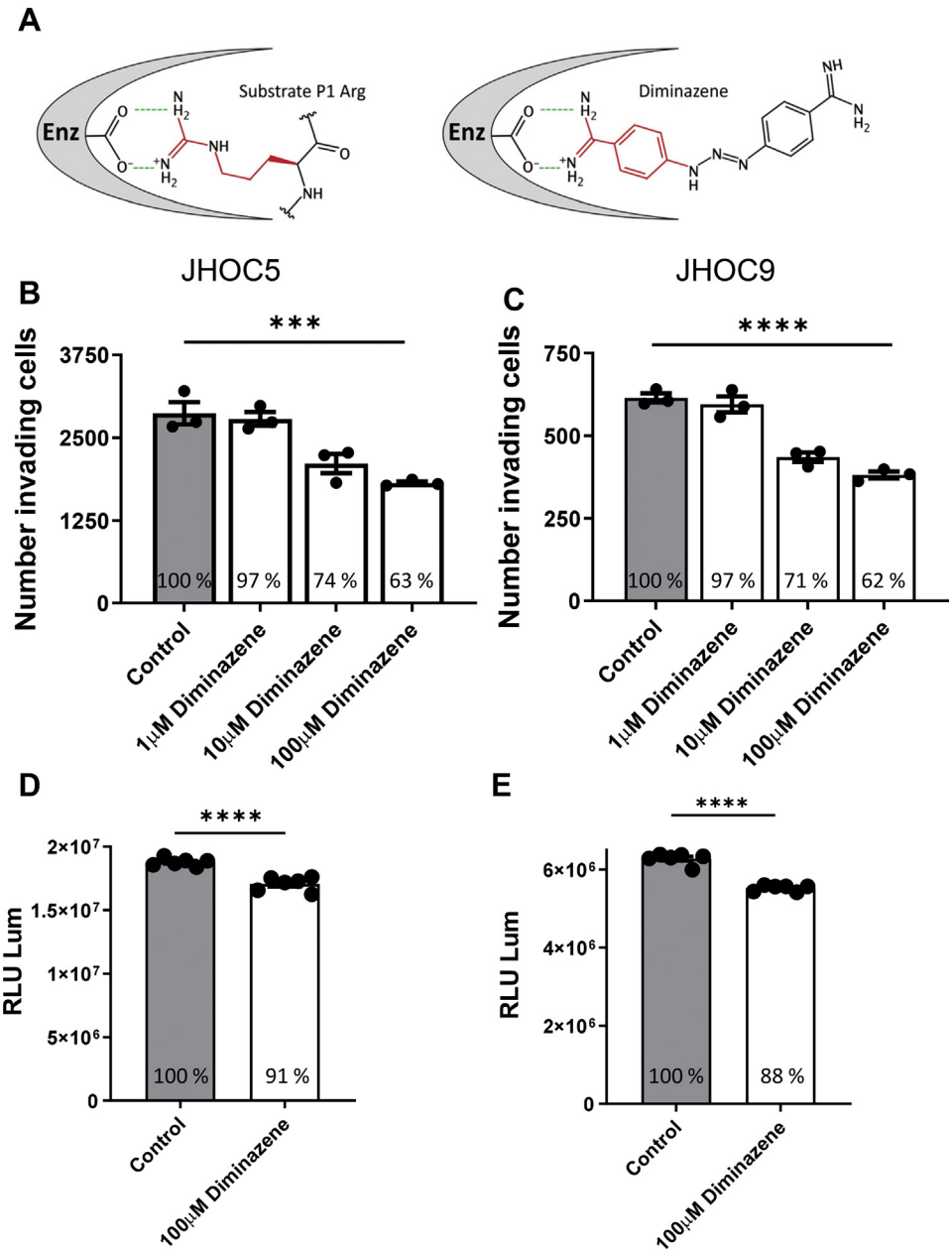

Figure 1. Tumor cell treatment with serine protease inhibitor diminazene implicates trypsin-like serine proteases in OCCC malignancy. *A*, depiction of serine protease interaction with Arg side chain of a substrate (*left panel*) *versus* the chemically similar competitive inhibitor diminazene (*right panel*). In either case, the positively charged guanidine or amidine moiety forms an ionic interaction with a negatively charged Asp side chain in the enzyme primary specificity pocket. *B* and *C*, treatment with diminazene significantly reduces tumor cell invasion in a concentration-dependent manner compared to vehicle-only control in JHOC5 (*B*) and JHOC9 (*C*) OCCC cell lines. *D* and *E*, treatment with diminazene significantly reduces proliferation compared to vehicle-only control in JHOC5 (*D*) and JHOC9 (*E*) cell lines. Invasion assay significance was calculated with ordinary one-way ANOVA. Post-hoc *t*-tests with Dunnett correction for multiple comparisons were also conducted; 10 μM and 100 μM (but not 1 μM) were significant for both. Proliferation significance was calculated with *t* test. Displayed within bar is the percentage relative to the control. ***$p < 0.001$, ****$p < 0.0001$. OCCC, ovarian clear cell carcinoma.

reasoned that trypsins are unlikely to be the relevant target(s) of the serine protease inhibitors that are responsible for promoting invasion and proliferation in OCCC. Rather, we hypothesized that alternative trypsin-like serine proteases targeted by diminazene, gabexate mesylate, and hydroxystilbamidine are expressed in active form in OCCC where they represent drivers of the observed malignant phenotypes.

Design and synthesis of an arginine diphenylphosphonate probe to label active trypsin-like serine proteases

There are 79 candidate trypsin-like serine proteases in the human proteome (Tables S1 and S2). Because they are typically regulated by posttranslational cleavage and by endogenous inhibitors, levels of transcript and protein expression often do not reflect levels of enzyme activity (5, 10, 11). To directly identify the most likely candidate enzymes based on

activity, we designed an activity-based probe with an arginine diphenylphosphonate warhead to target serine proteases with trypsin-like specificity as broadly as possible (Fig. 2*A*). Arg, rather than Lys, was selected for the warhead due to the observation that among 68 trypsin-like proteases with data for Arg *versus* Lys preference, 56 show marked preference for Arg but only one shows marked preference for Lys (Tables S1 and S2).

Because many serine proteases show greatly enhanced binding and activity toward substrates with compatible residues in extended subsites P_2 – P_4 (7), we incorporated the Arg diphenylphosphonate warhead into the sequence Ala-Ala-Pro-Arg. Proline was selected for the P_2 position because prior studies have shown Pro backbone angles to be compatible with the S_2 subsite but incompatible with S_1, S_3, and S_1' subsites of S1 family serine proteases; thus Pro in the P_2 position can favor productive binding and prevent nonproductive binding configurations (37, 38). P_2 Pro is strongly preferred by thrombin and is tolerated by other trypsin-like proteases for which extended specificities have been broadly profiled, including plasmin, uPA, factor Xa, KLK4, β-tryptase, matriptase, matriptase-2, matriptase-3, hepsin, HAT, and DESC (39–44).

These specificity profiling studies further demonstrate diverse but generally permissive specificity for P_3 and P_4 substrate residues. We selected alanine for these positions with the rationale that its small hydrophobic side chain could be widely accommodated without introducing steric clashes. The recognition sequence was incorporated as the C-terminal portion of the amino acid sequence GTENLYFQGGAAPR-diphenylphosphonate, which also contains a TEV protease cleavage site (ENLYFQ↓G). At the N-terminus of the peptide, a PEG linker serves as a spacer connecting a biotin tag used as an affinity handle (Fig. 2*A*). Solid phase peptide synthesis was completed using standard automated fluorenylmethyloxycarbonyl (Fmoc)/tert-butyl (tBu) chemistry followed by cleavage from the resin, solution phase coupling to (D/L) Arg(di-Boc)-diphenylphosphonate, deprotection, and purification of the final product.

The probe interaction with a protease is expected to initiate as a substrate-like interaction in which the Arg side chain

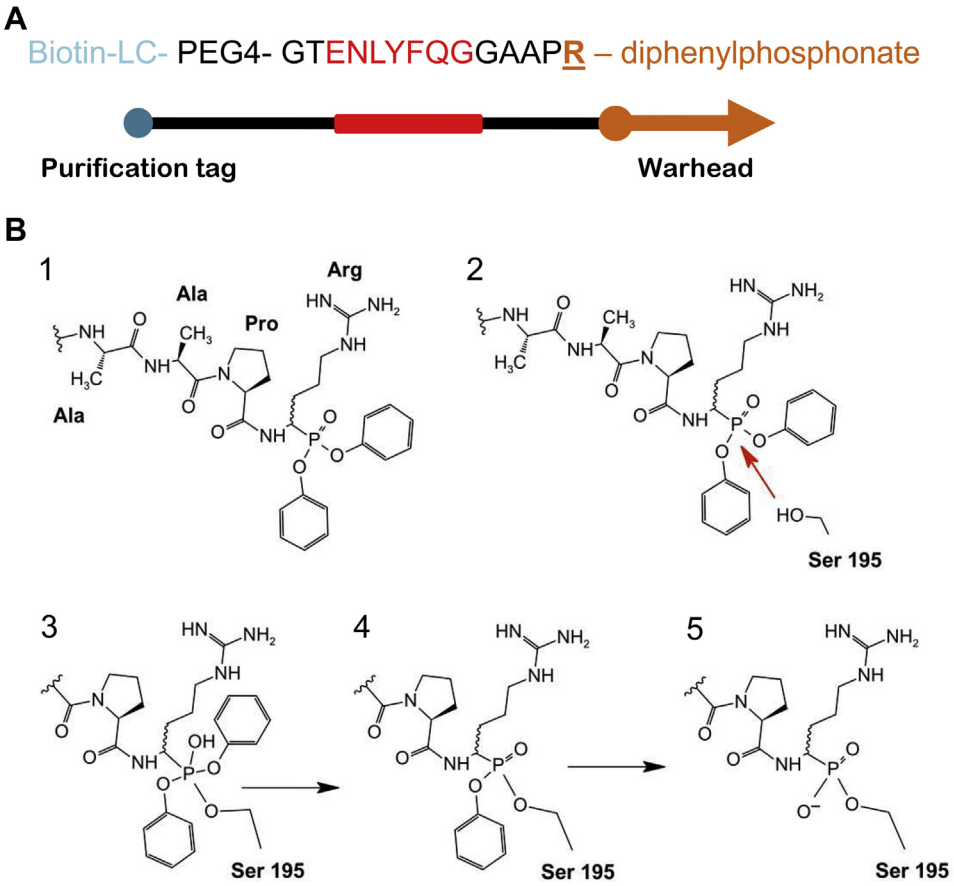

Figure 2. Design of activity-based probe targeting active trypsin-like serine proteases. *A*, schematic overview of the probe shows C-terminal warhead comprised of arginine diphenylphosphonate (*orange*) incorporated as the final residue of the GAAPR generic substrate recognition sequence that will bind in the catalytic cleft of a target protease. The substrate recognition sequence is preceded by a TEV-protease cleavage site (ENLYFQG, *red*) for optional release of a probe-labeled peptide. A PEG4 linker connects the long-chain (LC) biotin affinity handle (*blue*) to the peptide N-terminus. *B*, chemical structure and mechanism of protease labeling by reactive Arg diphenylphosphonate warhead. (1) Chemical structure of –AAPR-diphenylphosphonate warhead. (2) An active trypsin-like serine protease initiates nucleophilic attack by the catalytic serine (Ser-195 according to chymotrypsin family canonical numbering) at the phosphate center of the diphenylphosphonate. (3) A covalent bond is established between the probe phosphonate and the protease active site Ser, resulting in a pentacoordinate transition state. (4) An initial adduct is formed by displacement of phenol. (5) Aged adduct may result upon loss of the remaining phenyl ring.

occupies the primary specificity pocket. Upon nucleophilic attack by the enzyme serine nucleophile on the phosphorus center of the diphenylphosphonate, the complex is expected to proceed through a pentacoordinate transition state leading to a stable covalent adduct with displacement of phenol (16, 45) (Fig. 2*B*). Based on prior studies of similar covalent inhibitors, it is anticipated that over time, an aged adduct may emerge upon loss of the second phenyl ring (18, 46).

Probe characterization verifies Ser195 specific labeling of a model catalytically active protease

We characterized the anticipated probe-protease behavior using active mesotrypsin, a human trypsin isoform, compared to a catalytically inactive mesotrypsin-S195A mutant lacking the reactive serine nucleophile. Both mesotrypsin and the S195A mutant were incubated with the probe and then samples were subjected to Western blotting to detect the biotin handle with horseradish peroxidase–conjugated streptavidin. The results showed a clear and intense band at the approximate gel mobility of mesotrypsin for the WT protein. In contrast, no signal was detected in the S195A mutant sample, demonstrating the specificity for labeling of the active site serine by the probe (Fig. 3*A*, loading control Fig. 3*B*). We further found that the active site modification by the probe was quantitative and complete, by using an activity assay with a colorimetric peptide substrate of mesotrypsin. Whereas untreated WT mesotrypsin demonstrated high turnover of the substrate, a comparable concentration of mesotrypsin incubated with the probe showed almost no residual catalytic activity (Fig. 3*C*). This assay further verified the specific and complete targeting of the active site serine 195 by the ABPP probe, resulting in elimination of catalytic activity.

Using mass spectrometry, we next queried the total mass difference of intact mesotrypsin modified by the probe compared to unmodified mesotrypsin. The spectra revealed a mass shift of 2160.06 Da between the test samples, within experimental tolerance of the calculated mass addition of 2160.53 Da expected for labeling with 1 mol equivalent of the probe to yield the monophenoxyphosphonyl derivative (Figs. 3, *D* and *E* and S4). As a control, we also incubated the mesotrypsin-S195A mutant with the probe and compared the resulting spectrum to that obtained from an untreated control sample. We did not detect any labeling of the catalytically inactive mesotrypsin-S195A mutant *via* mass spectrometry, confirming the high specificity of the probe for the active site Ser-195 (Fig. S5).

Despite the clear evidence of quantitative labeling of active mesotrypsin by the probe, initial efforts to directly detect probe labeling of Ser-195 in MS/MS sequencing of trypsin/TEV protease digests of probe-treated mesotrypsin were unsuccessful, instead revealing the unlabeled form. Further investigation revealed that the covalent probe adduct was unstable to standard mass spectrometric higher-energy collisional dissociation (HCD) fragmentation, which preferentially fragmented the probe from the peptide (Fig. S6). Subsequent modification of the MS/MS protocol to employ the softer electron transfer dissociation (ETD) fragmentation approach

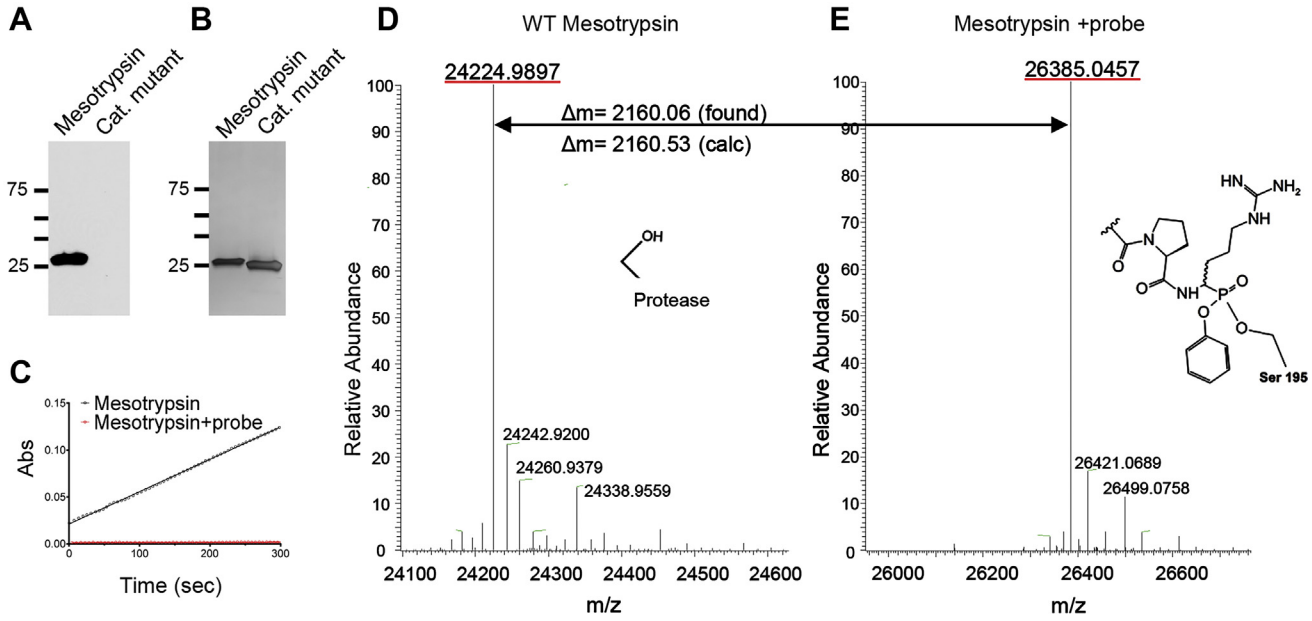

Figure 3. Validation of the activity-based probe using mesotrypsin as a target protease. *A*, efficiency and specificity of the probe for labeling the catalytic serine of a trypsin-like protease was tested using catalytically active mesotrypsin compared to a catalytically inactive mesotrypsin-S195A mutant. Recombinant proteases were incubated for 1 h with the probe (4 μM protease:16 μM probe) and then analyzed using Western blotting; the biotin tag was detected using HRP-conjugated streptavidin. A strong signal was observed for probe-labeled active mesotrypsin with no detectable signal for the S195A mutant (2 ng protein per lane). *B*, silver-stained gel run in parallel with the same samples demonstrates equivalent protein concentrations (1 μg protein per lane). *C*, activity assay using chromogenic substrate Z-GPR-pNA shows substrate turnover by active mesotrypsin incubated with vehicle control (*black line*), whereas active mesotrypsin preincubated with the probe reveals complete inhibition of activity (*red line*). *D*, mass spectrum of intact mesotrypsin reveals a major mass peak of 24224.9897 Da. *E*, after incubation with the probe, the mass peak is shifted by addition of 2160.06 Da, within the experimental tolerance of the calculated mass addition expected for labeling with 1 mol equivalent of the probe to yield the monophenoxyphosphonyl derivative.

ultimately led to successful detection of fragment ions deriving from probe-labeled mesotrypsin, directly confirming the site of probe labeling as the active site Ser-195 (Fig. S7).

Activity-based probe detects secreted active trypsin-like serine proteases in OCCC cell cultures

Following the characterization of the probe, we developed and optimized a standardized workflow for probe labeling of secreted active proteases in cell culture. We focused on the secreted proteome because most trypsin-like serine proteases are secreted enzymes, with the remaining few being extracellularly displayed transmembrane proteases that are shed from the cell surface through proteolysis (47) (Tables S1 and S3). Cells were cultured for 24 h in a minimal volume of serum-free media with exposure to the probe during the final hour, followed by clarification and concentration of the conditioned media. The secreted proteome was recovered by methanol/chloroform precipitation to eliminate excess unreacted probe and then resolubilized. Labeled proteins were then captured *via* the biotin affinity handle using streptavidin coated beads, resolved by SDS-PAGE, and captured proteins were analyzed by tandem MS/MS protein identification (Fig. 4*A*). We examined two OCCC cell lines using this workflow, JHOC5 and JHOC9, with the aim to query their complex proteomes for secreted active serine proteases and to identify as candidate mediators of malignancy the active proteases present in both models. Western blot analysis detecting the biotin adduct revealed three distinct bands for analysis in the JHOC5-conditioned media proteome (Fig. 4*B*). The JHOC9 proteome displayed evidence of labeled proteins across a broader spectrum of molecular weights, from which we chose the four most intense bands for analysis (Fig. 4*D*). Bands of corresponding gel mobility excised from duplicate silver stained gels (Fig. 4, *C* and *E*) were analyzed using mass spectrometry. We identified two trypsin-like serine proteases that were present in both OCCC cell lines: tPA and uPA (Tables 1 and 2). In the JHOC9 cell line, we identified a number of additional proteases: kallikrein 6 (KLK6), 10, and 13, and transmembrane protease serine 11F (Table 2). Taken together, we detected common and unique active proteases in the two OCCC cell lines and next proceeded to interrogate the candidates identified in common for their role in tumor progression.

Serine proteases uPA and tPA identified by ABPP promote OCCC cell invasion and proliferation

Focusing on the two active proteases that were detected in both JHOC5 and JHOC9 cells, we next conducted experiments to assess the potential contributions of these enzymes to OCCC malignancy and further define their expression and activity in OCCC models. The serine protease uPA, also known as urokinase, contributes to the activation of plasminogen to plasmin, a process involved in clot lysis, wound healing, and tissue remodeling. Previous work has shown that uPA can also be a driver of malignancy, and its expression has been linked to poor prognosis in multiple tumor types (48, 49). To assess the relevance of uPA for tumor cell malignancy in OCCC, both cell lines were subjected to lentiviral shRNA gene silencing targeting the *PLAU* gene. We found that knockdown of *PLAU* using two different lentiviral constructs (Fig. 5, *A* and *B*) significantly impaired cellular invasion through artificial basement membrane in a standard Boyden chamber assay (Fig. 5, *C* and *D*). Additionally, knockdown of *PLAU* significantly impaired tumor cell proliferation compared to the control in both JHOC5 and JHOC9 cells (Fig. 5, *E* and *F*).

We next examined presence and susceptibility to activity-based labeling of different uPA protein species in JHOC9 cultures, since this model had shown most robust detection of uPA in proteomic analyses (Fig. 4*D* and Table 2). Cultures transfected with a control nontarget lentivirus or with a *PLAU*-targeted knockdown lentivirus were labeled with the activity-based probe, and then conditioned medium was analyzed directly on Western blots with detection for uPA or for the biotinylated probe. Two uPA species were detected with anti-uPA antibody, a major band representing the single-chain mature zymogen (~49 kDa) and a minor band representing the beta-chain of proteolytically activated uPA containing the catalytic domain (~30 kDa) (Fig. 6*A*). Both bands were completely absent from the *PLAU* knockdown culture, confirming the efficacy of knockdown at the protein level. Detection with streptavidin revealed labeling of the 30 kDa band coinciding with the catalytically active beta-chain; absence of this band in the knockdown sample further supports its identification as active uPA (Fig. 6*A*). No streptavidin signal was observed coincident with the 50 kDa zymogen, consistent with specificity of the activity-based probe toward proteolytically activated uPA; the very low basal level of activity that has been reported for the single-chain zymogen (50) was insufficient for reactivity with the probe.

To evaluate the potential of our activity-based probe for interrogating the more complex proteome of the tumor microenvironment *in vivo*, we conducted a labeling experiment using ascites fluid collected from tumor-bearing mice. We have previously established the JHOC9 intraperitoneal injection model to recapitulate processes occurring during intraperitoneal metastasis of OCCC (51). Incubation of ascites fluid collected from mice-bearing JHOC9 tumors with our activity-based probe resulted in detection of several labeled protein bands including the 30 kDa band also identified by anti-uPA antibody (Fig. 6*B*), confirming the relevance of this active protease species *in vivo*.

Like uPA, tPA is also an activator of plasmin, with roles in regulation of fibrinolysis; however, the role of this protease in cancer is much less clear and may vary by tumor type. To investigate the significance of tPA for hallmarks of malignancy in OCCC, we used lentiviral shRNA constructs against tPA to knockdown the *PLAT* gene in both OCCC cell lines (Fig. 7, *A* and *B*), and cells were tested for the ability to invade through artificial basement membrane and to proliferate. Similarly to cells with *PLAU* knockdown, following *PLAT* knockdown, we found significant reduction of both invasive capability (Fig. 7, *C* and *D*) and proliferation (Fig. 7, *E* and *F*) compared to the controls in both cell lines. To further explore the specificity of these phenotypic effects, we also examined the impact of

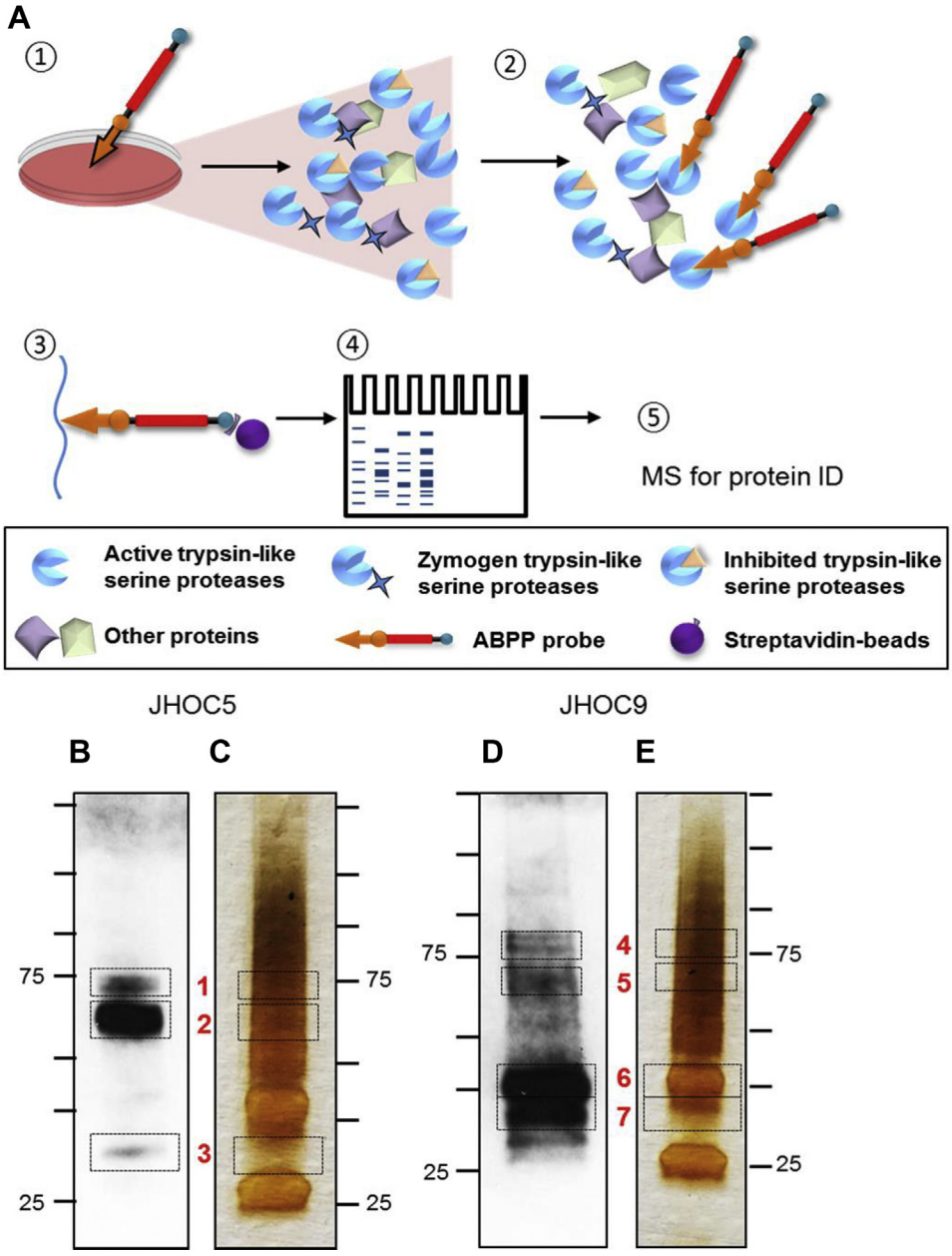

Figure 4. Labeling of active trypsin-like serine proteases in cell culture using activity-based probe. *A*, scheme of labeling workflow. (1) Cells were cultured to high confluency and the probe was added directly to the culture medium to modify only the active trypsin-like serine proteases while leaving zymogen forms, inhibited complexes, or otherwise inactive protease forms unlabeled (2). (3) Using the biotin affinity handle, magnetic streptavidin beads were used to purify the probe-labeled proteins. (4) Samples were then further purified and visualized using SDS-page separation, followed by (5) protein identification using MS. *B–E*, Western blots probed with HRP-conjugated streptavidin identified signal for multiple biotinylated bands, potentially representing labeled active proteases, from both the JHOC5 (*B*) and JHOC9 (*D*) cultures. Bands in rectangles (*gray*), chosen for further analysis, were excised from duplicate silver-stained gels run in parallel (*C* and *E*) and subjected to in-gel digestion followed by LC-MS/MS (see Tables 1 and 2).

silencing KLK-6, a serine protease that was identified by probe labeling in JHOC9 cells but not in JHOC5 cells. RT/PCR showed that *KLK6* transcripts were robustly expressed in JHOC9 cells but not detected in JHOC5 cells, consistent with proteomic results. Unlike our findings with uPA and tPA, however, silencing of KLK-6 in JHOC9 cells did not have any

Table 1
Enriched and identified active serine proteases in JHOC5 OCCC cells

Protein	Band	kDa	-10lgP (threshold)	Coverage (%)	#Unique
Tissue-type plasminogen activator (tPA)	1	68	126.51	17	11
	2		167.25	33	23
Urokinase-type plasminogen activator (uPA)	3	49	86.3	13	7

Table 2
Enriched and identified active serine proteases in JHOC9 OCCC cells

Protein	Band	kDa	-10lgP (threshold)	Coverage (%)	#Unique
Tissue-type plasminogen activator (tPA)	4	68	49.9	2	1
	5		115.48	18	11
Transmembrane protease serine 11F	5	50	25.64	8	2
Kallikrein-6	6	27	120.75	22	4
	7		122.58	24	9
Kallikrein-10	6	30	168.57	38	10
	7		147.8	31	14
Kallikrein-13	6	31	217.94	55	17
	7		132.61	31	10
Urokinase-type plasminogen activator (uPA)	6	49	181.42	23	11
	7		124.38	24	14

significant effects on invasion or proliferation (Fig. S8), thus highlighting the specific impact of uPA and tPA on these malignant phenotypes.

We next directly examined tPA protein species and susceptibility to probe labeling in JHOC5 cultures, where tPA had been most robustly detected in proteomic results (Fig. 4*B* and Table 1). Atypically for a serine protease, single-chain tPA possesses most of the enzymatic activity of the cleaved two-chain form; the activating cleavage, catalyzed by its product plasmin in a positive feedback loop, increases the activity of tPA only modestly (52, 53). Conditioned medium from the probe-labeled control culture showed a band detected by anti-tPA at ~68 kDa, consistent with the expected size of single-chain tPA (Fig. 8*A*); no two-chain tPA was detected. This band was also labeled by the activity-based probe, demonstrating that the activity of single-chain tPA is sufficient for reactivity with this probe. The band was absent in samples from the *PLAT*-knockdown culture (Fig. 8*A*), further confirming the band identity as tPA and demonstrating the efficacy of the knockdown at the protein level.

We also evaluated the presence and probe reactivity of tPA in ascites samples collected from tumor-bearing mice from our previously established JHOC5 intraperitoneal injection model of OCCC (51). The 68 kDa band was detected by anti-tPA in all available ascites samples and was strongly labeled by the activity-based probe as indicated by streptavidin staining (Fig. 8*B*), confirming the significant presence of this reactive species in the tumor microenvironment. The corroboration of both uPA and tPA protein expression, activity, and probe labeling in ascites samples from tumor-bearing mice (Figs. 6*B* and 8*B*) suggests that these mediators of malignancy are indeed relevant to the *in vivo* setting. These results further highlight the potential utility of our probe for directly interrogating complex tumor microenvironments.

Altogether, our data identify uPA and tPA as mediators of OCCC growth and progression, suggesting possible points of therapeutic intervention and provide an example illustrating how our activity-based probe can successfully identify trypsin-like serine proteases of interest in biological model systems.

Discussion

The advent of gene expression analysis and fast progress in the field of genomics have led to increased understanding of how genetic mutations and transcriptional changes predispose to disease (54, 55). There remains, however, a knowledge gap between the transcriptome and the functional proteome, as protein activity is shaped by posttranslational regulation through covalent modification, limited proteolysis, and interactions with activity-modifying ligands and binding partners. Differences between transcript abundance, protein abundance, and protein activity can be particularly stark for proteases, given their multiple layers of posttranslational regulation. Proteases are typically produced as zymogen precursors that persist as latent enzymes until activation by limited proteolysis (56, 57). Once activated, levels of protease activity may be further influenced by covalent modifications including phosphorylation (58) and by ligand binding to allosteric regulatory sites (59, 60). Finally, activated proteases are often coexpressed and colocalized with very tight binding protein protease inhibitors (61, 62), further titrating their actual availability to catalyze proteolytic reactions. Unsurprisingly in light of these mechanisms of regulation, it is often the case that the overwhelming majority of a protease in its biological context is present in various inactive forms. Whereas both transcriptional readouts and traditional proteomics approaches will thus fail to give an accurate picture of the protease landscape in terms of activity, an activity-based proteomic approach can address this need and identify catalytically active proteases in highly complex proteomes. The present study highlights the capability of such an activity-based approach, as we successfully detected proteases that were directly involved as drivers of malignancy in OCCC cell lines.

Some of the earliest applications of ABPP focused on the large group of serine hydrolases (63), of which nearly half have currently uncharacterized function (64). ABPP methods were easily recruited to target these enzymes, facilitated by a conserved enzyme mechanism featuring a nucleophilic serine that forms a covalent intermediate by attacking a substrate electrophilic center. Activity-based probes were designed with highly electrophilic and reactive warheads that undergo nucleophilic attack by serine to form stable adducts, thus detecting a plethora of serine hydrolase targets including lipases, esterases, amidases, and serine proteases (64). Warhead design initially exploited relatively promiscuous fluorophosphonates as the preferred electrophile. Such an

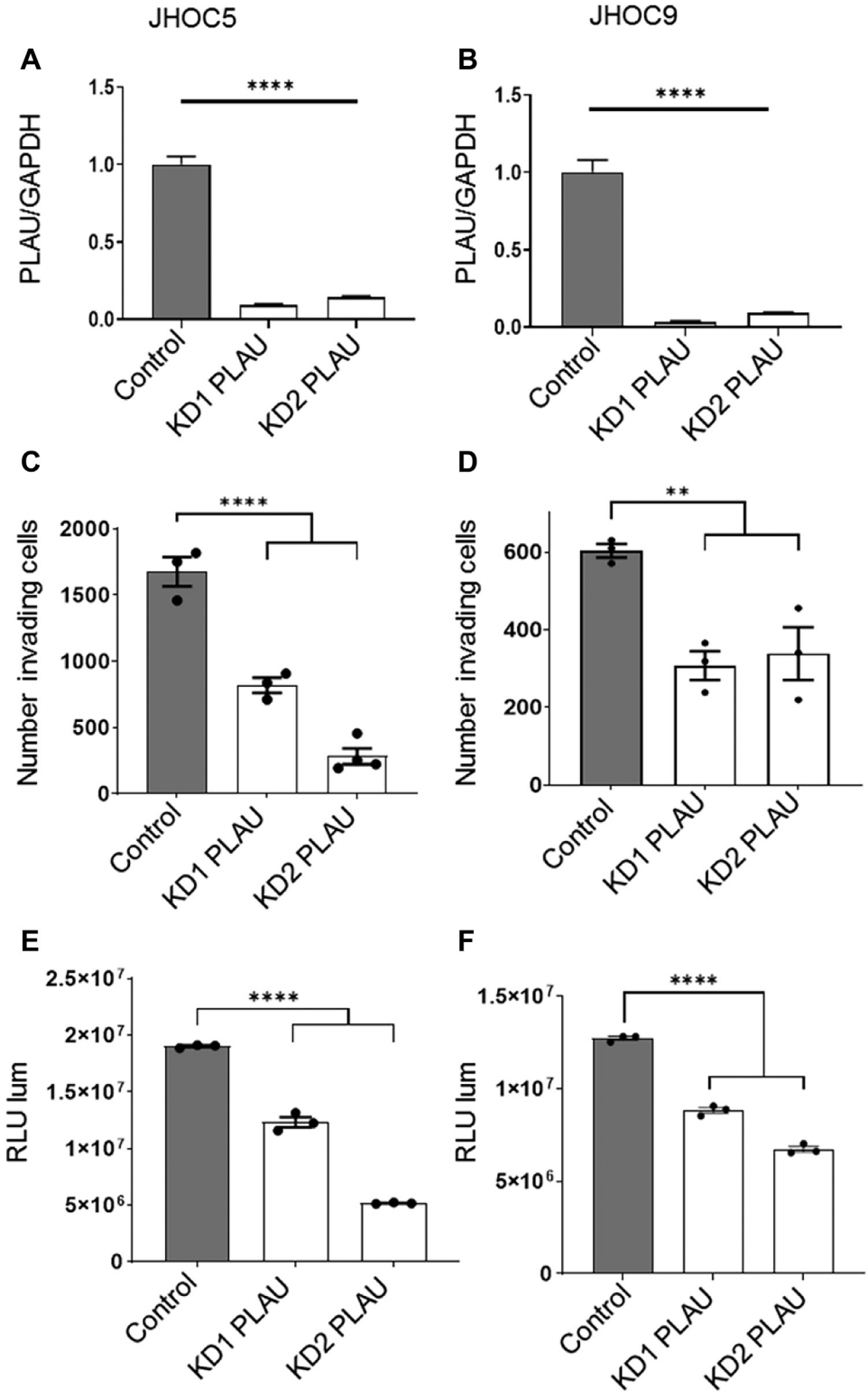

Figure 5. Tumor cell–expressed urokinase-type plasminogen activator (uPA) drives malignant phenotype in OCCC. *A* and *B*, expression of *PLAU*, the gene encoding uPA, was efficiently silenced using two independent lentiviral shRNA constructs in OCCC cell lines JHOC5 (*A*) and JHOC9 (*B*). *C* and *D*, silencing of *PLAU* significantly impaired tumor cell invasion in Matrigel transwell assays of JHOC5 cells (*C*) and JHOC9 cells (*D*) compared to controls. *E* and *F*, silencing of *PLAU* significantly impaired tumor cell proliferation as reflected in viability assays of JHOC5 cells (*E*) and JHOC9 cells (*F*) compared to controls. Significance assessed with one-way ANOVA; $^{**}p < 0.01$, $^{****}p < 0.0001$. OCCC, ovarian clear cell carcinoma; uPA, urokinase-type plasminogen activator.

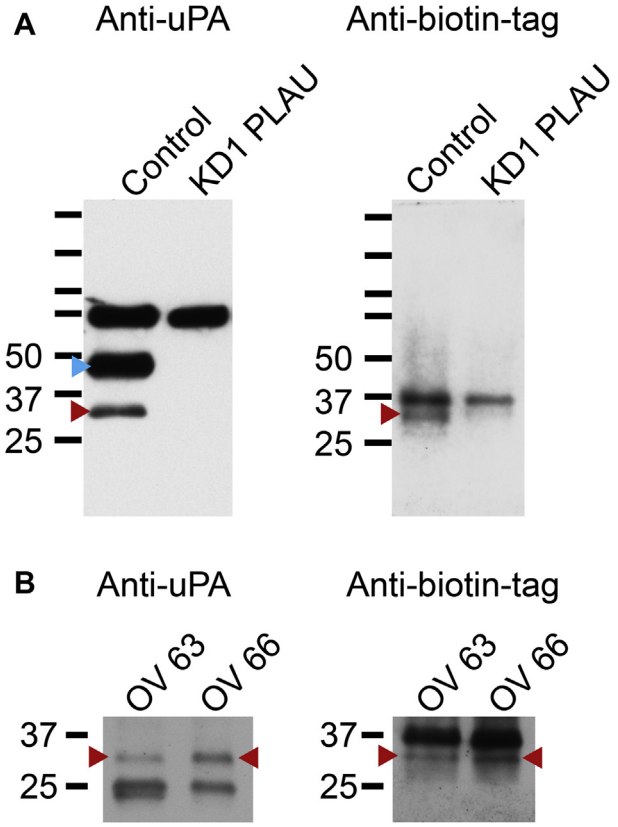

Figure 6. uPA protein labeling with activity-based probe in cell lysates and in malignant ascites samples. *A*, JHOC9 control cultures and cultures subjected to *PLAU* knockdown were labeled with the activity-based probe, and then conditioned media were analyzed by Western blotting. Anti-uPA detection (*left panel*) revealed both the uPA single-chain zymogen (*blue arrow*) and the 30 kDa beta-chain of activated uPA (*red arrow*) in the control sample; both bands were eliminated by *PLAU* knockdown. Note that the extra band detected by the uPA antibody at 75kD is nonspecific as demonstrated by its presence in the KD sample. Streptavidin detection of the biotin tag (*right panel*) reveals probe labeling of the 30 kDa active form of uPA that is present in control but not knockdown sample (*red arrow*); the zymogen form of uPA is not labeled, demonstrating probe specificity. *B*, malignant ascites fluid, retrieved from two mice carrying intraperitoneal JHOC9 tumors, was incubated with the activity-based probe and then analyzed by Western blotting. Anti-uPA (*left panel*) detected the 30 kDa active uPA protein form (*red arrow*) and streptavidin detection (*right panel*) confirmed probe-labeling of this species in both samples. uPA, urokinase-type plasminogen activator.

activity-based probe against serine hydrolases was used to demonstrate that MDA-MB-231 breast cancer cells implanted *in vivo* show differential hydrolase activity that is influenced by the host stroma, including striking increases in activity of both tPA and uPA (65). Use of a similar probe identified the lipolytic enzyme monoacylglycerol lipase as highly expressed in cancer cells and discovered its function as a liberator of free fatty acids within tumor cells, which in turn are used as an energy source and lead to increased tumor cell survival and proliferation (66). Most recently, Wang *et al.* (67) have synthesized a series of probes with alternative substituted phenylphosphonate warheads to fine-tune selectivity toward different subsets of intracellular serine hydrolases, in addition making use of a shorter linker and CuAAC click-chemistry to produce highly cell permeable probes.

A smaller subset of serine hydrolases can be more specifically interrogated by probes with a diphenylphosphonate-containing warhead, which reacts more uniquely with serine proteases. Irreversible serine protease inhibitors featuring this functional group were pioneered by Powers *et al.* (16, 45) and subsequently adapted as fluorescent probes (17, 26) or attached to biotin for affinity isolation and identification of serine proteases (19, 25). Optimization of peptide amino acid sequence has led to inhibitors of enhanced selectivity toward individual serine proteases, such as granzymes A and K (18). Joosens *et al.* (23) enhanced selectivity toward uPA further by employing a guanidinylated benzyl diphenylphosphonate group instead of the natural lysine or arginine at the P_1 position and additionally optimizing the P4 position. Here, we aimed instead to more broadly target the trypsin-like serine proteases, which critically house within the S1 specificity pocket either aspartic acid or glutamic acid, leading to substrate specificity for peptide cleavage after lysine or arginine. We chose to design the probe with a diphenylphosphonate warhead with arginine in the P_1 position, as preferred by the great majority of human trypsin-like proteases in the MEROPS database (Tables S1 and S2) (4) and additionally to populate the P_2-P_4 positions with an extended recognition motif well tolerated by many serine proteases. This probe design was validated by our labeling and identification of a variety of trypsin-like serine proteases secreted by JHOC5 and JHOC9 OCCC cell lines.

While the Ala-Ala-Pro-Arg recognition motif was designed to be broadly reactive with trypsin-like serine proteases, reactivity with individual proteases may vary according to their individual substrate specificities at the P_1–P_4 subsites. It is possible that we may have failed to capture and detect some active secreted trypsin-like proteases either due to low abundance or because they were poorly reactive with the extended subsite residues of the probe design. In future work, it may be possible to achieve enhanced sensitivity with this or similar probes by adapting our methodology to a gel-free proteomic workflow. Our probe further incorporated a tandem orthogonal proteolysis design, first described by Speers *et al.* (27), which allows for interrogation of the labeled protein as well as the site of labeling by sequential digestion with trypsin and TEV protease and offers potential advantages for sensitivity and specificity of detection. It may be feasible to modify our probe for intracellular labeling by substituting the TEV recognition site, linker and biotin for the smaller alkyne functionality, and employing click chemistry to introduce these elements after labeling, thus further extending the reach of the method (28).

Our findings included the discovery that zymogen and activated uPA are secreted by OCCC cell lines, where uniquely the activated form was detected by our activity-based probe. The physiological role of uPA is the activation of plasminogen to plasmin, a pivotal serine protease that degrades many extracellular matrix components during tissue remodeling and activates zymogen forms of other enzymes including matrix metalloproteinases (48, 68, 69). Both plasmin and matrix metalloproteinases have been implicated in cancer, and uPA as a major activator has drawn interest for its role in cancer development and progression with emphasis on metastatic spread (48, 49, 70). In ovarian cancer, uPA is widely

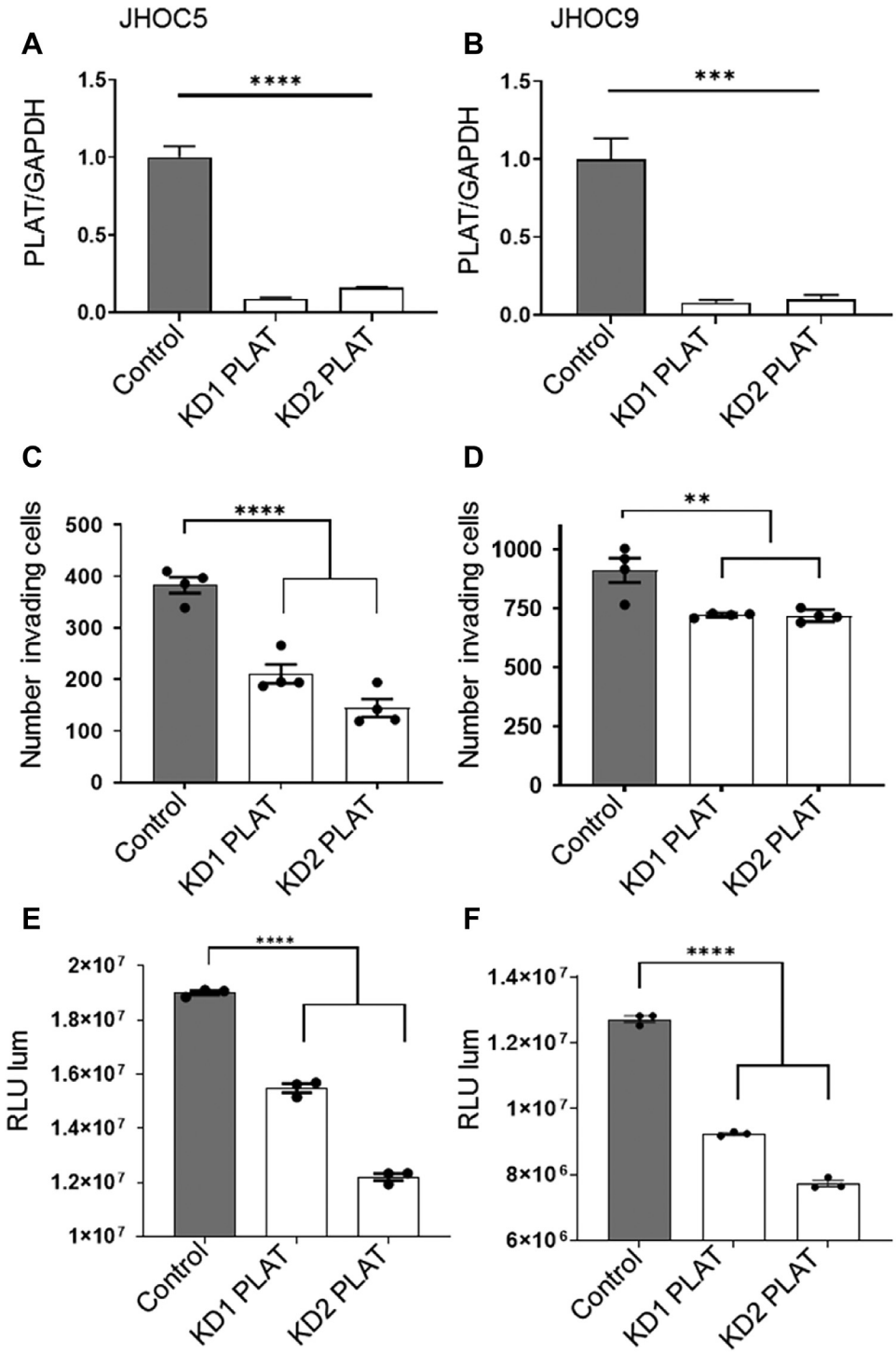

Figure 7. Tumor cell–expressed tissue-type plasminogen activator (tPA) drives malignant phenotype in OCCC. *A* and *B*, expression of *PLAT*, the gene encoding tPA, was efficiently silenced using two independent lentiviral shRNA constructs in OCCC cell lines JHOC5 (*A*) and JHOC9 (*B*). *C* and *D*, silencing of *PLAT* significantly impaired tumor cell invasion in Matrigel transwell assays of JHOC5 cells (*C*) and JHOC9 cells (*D*) compared to controls. *E* and *F*, silencing of *PLAT* significantly impaired tumor cell proliferation as reflected in viability assays of JHOC5 cells (*E*) and JHOC9 cells (*F*) compared to controls. Significance assessed with one-way ANOVA; $^{**}p < 0.01$, $^{***}p < 0.001$, $^{****}p < 0.0001$. OCCC, ovarian clear cell carcinoma; tPA, tissue plasminogen activator.

overexpressed by tumors and associated with progression and poorer outcomes (69, 71). It has been shown to facilitate tumor cell proliferation (72), invasion (73), and metastasis (74), effects that are dependent on uPA interaction with the cell surface urokinase plasminogen activator receptor (uPAR). This interaction can be inhibited by specific uPAR antibodies (74) or soluble uPAR (72), providing a possible means of therapeutic intervention. Furthermore, an intricate interplay between uPA, uPAR, and integrins including αvβ3 has been shown to be involved in the regulation of tumor cell invasion (75). Although less has been known about the potential involvement of these mechanisms in the progression of OCCC specifically,

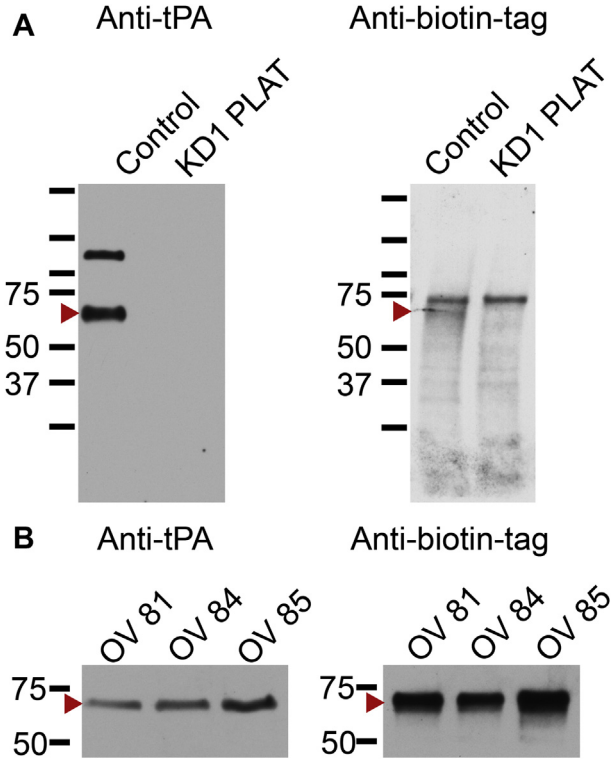

Figure 8. tPA protein labeling with activity-based probe in cell lysates and in malignant ascites samples. *A*, JHOC5 control cultures and cultures subjected to *PLAT* knockdown were labeled with the activity-based probe, and then conditioned media were analyzed by Western blotting. Anti-tPA detection (*left panel*) identified a clear band at the expected size for single-chain tPA (*red arrow*) in the control sample; no band is detected after *PLAT* knockdown. Streptavidin detection of the biotin tag (*right panel*) reveals faint probe-labeling of single-chain tPA in the control sample (*red arrow*) while this band is absent in the knockdown sample. *B*, malignant ascites fluid, retrieved from three mice that carried intraperitoneal JHOC5 tumors, was incubated with the activity-based probe and then analyzed by Western blotting. Anti-tPA (*left panel*) detected a band for single-chain tPA protein; this band was also very strongly detected by streptavidin (*right panel*), confirming robust probe-labeling of this species in all three samples. tPA, tissue plasminogen activator.

our present findings demonstrate uPA to promote both OCCC cell proliferation and invasion, implicating uPA as a significant driver of tumor growth and progression in OCCC.

We also identified single-chain tPA as an active protease secreted by OCCC cells. As a plasminogen activator, tPA is a primary mediator of fibrinolysis and thrombolysis in the vascular system through generation of active plasmin; it has also been widely used in recombinant form as a therapy to lyse clots in acute ischemic stroke (76). Single-chain tPA possesses significant basal activity and is further allosterically stimulated *via* binding to fibrin at sites of blood clots (52). In our experiments using OCCC cell culture medium, tPA basal activity was sufficient for activity-based probe labeling (Fig. 8*A*). Notably, however, we did observe markedly more intense probe labeling of tPA in complex ascites samples (Fig. 8*B*), which might be explained from prior observations of human ovarian cancer and mouse models showing influx of fibrinogen and accumulation of fibrin degradation products in ovarian cancer ascitic fluid (77–79). Thus, allosteric stimulation of tPA activity in ascites by incompletely digested fibrin fragments may enhance reactivity with our activity-based probe; this possibility will require further investigation.

The role of tPA has been little studied in most forms of cancer, but substantive data support a malignancy promoting role for tPA in pancreatic cancer and glioma. In pancreatic cancer models, tumor cell expression of tPA was shown to promote cell proliferation and tumor growth through mechanisms involving epidermal growth factor signaling (80, 81). It has also been found to promote pancreatic cancer cellular invasion *via* binding to cell surface receptor annexin II and mediating localized activation of plasminogen to plasmin (82, 83). In glioma, tPA has been implicated as a key factor in malignancy, since its knockdown in glioma-initiating cells, or its downregulation by miRNA-340, inhibits both proliferation and invasion *in vitro* and tumor growth *in vivo* (84). While the potential significance of tPA in ovarian cancer previously has not been a major focus of study, the present study implicates tPA along with uPA as a driver of invasion and proliferation in OCCC. Our work suggests that both of these plasminogen activators, along with downstream pathways activated in common by these enzymes (69), may represent potential targets in OCCC. Additional work is needed to identify the most effective therapeutic approach to reduce the protumorigenic effect of both uPA and tPA.

In summary, we show that our arginine diphenylphosphonate activity–based probe can successfully profile serine protease activity in a complex secreted proteome. Interrogation of OCCC cells resulted in the detection of multiple target proteases for which we demonstrate active involvement in malignant phenotypes that contribute to cancer growth and progression. Together, our findings highlight the potential uses for ABPP in the rapidly expanding field of proteomics to aid in the identification of therapeutic targets and guide the future development of targeted therapy.

Experimental procedures

Activity-based probe design and synthesis

The activity-based probe was custom synthesized in collaboration with Peptides International (Cat# PCS-31822-PI, Lot# 003066C, formula $C_{103}H_{152}N_{23}O_{30}SP$).

Solid phase synthesis

Biotin-[NH-(CH2)5-COO]-dPEG4-Gly-Thr(tBu)-Glu-Asn(Trt)-Leu-Tyr(tBu)-Phe-Gln(Trt)-Gly-Gly-Ala-Ala-Pro-OH was synthesized (0.4 mmol scale) by standard automated (Prelude, Protein Technology Inc) Fmoc/tBu chemistry using a solid support H-Pro-2-ClTrt resin (substitution: 0.58 mmol/g). The coupling of the amino acids in dimethylformamide (DMF) was carried out with diisopropyl carbodiimide and oxima in DMF activation chemistry for 3 h. The Fmoc group was removed by treating the peptide resin with 20% piperidine/DMF (2×, 2 min and 20 min each). The resin was thoroughly washed with DMF, dichloromethane, and methanol and dried to obtain a constant weight. The dried peptide resin was then cleaved with 1% TFA in dichloromethane (3×, 30 min each). The resin was filtered off

and the filtrate was evaporated and the residue was triturated with isopropyl ether. The protected peptide was centrifuged, washed with isopropyl ether (2×), and dried under high vacuum.

Solution phase coupling

The protected peptide and 1-Hydroxy-7-azabensotriazole were dissolved in DMF, and diisopropyl carbodiimide, (D/L) Arg(di-Boc)-diphenylphosphonate (Peptides International), and N-methylmorpholine were added. After 18 h, the reaction was completed and the peptide was precipitated by adding H_2O and washed two times with isopropyl ether, after which the solid material was dried under vacuum.

Final cleavage, purification, and validation

Complete cleavage of the protecting groups was carried out with a cleavage cocktail containing TFA (87.5%), triisopropylsilane (2.5%), H_2O (5.0%), and anisole (5%). After 3 h at ambient temperature, the product was precipitated with isopropyl ether, washed with isopropyl ether (3×), and dried under vacuum. The peptide was then purified by using a C-18 reversed phase column and characterized by LC-MS. The average molecular weight was determined to be 2255.53, and the probe showed 92.6% purity of the racemic mix of D + L isomers as determined by HPLC.

Expression of recombinant mesotrypsin and catalytically inactive mesotrypsin-S195A

Recombinant human mesotrypsin and catalytically inactive mutant mesotrypsin-S195A were expressed as zymogen precursors in *Escherichia coli*, isolated from inclusion bodies, refolded, purified by ecotin affinity chromatography, proteolytically activated using bovine enteropeptidase, and purified by benzamidine affinity chromatography as described previously (85). Enzyme concentrations were routinely measured by Nanodrop (NanoDrop One Thermo Scientific) using a calculated extinction coefficient at 280 nm of 41,535 M^{-1} cm^{-1}.

Western blot to detect probe labeling of mesotrypsin

Lyophilized aliquots of the activity-based probe were reconstituted in 25 μl dimethyl sulfoxide (DMSO) to make a stock concentration of 17 mM. Catalytically active mesotrypsin or the catalytically inactive mutant mesotrypsin were incubated at a concentration of 4 μM with 4-fold molar excess of the probe for 1 h at 37 °C, in a final volume of 100 μl in serum-free, phenol red–free Dulbecco's modified Eagle's medium (DMEM)/F12 media (Cat 21041025, Gibco). Following the incubation, samples were run under denaturing conditions on a 4 to 20% gradient SDS-PAGE (BioRad). Protein was transferred (20% methanol transfer buffer) onto nitrocellulose membrane. Following the transfer, the membrane was blocked for 1 h in 5% bovine serum albumin (BSA) TBST. Streptavidin-HRP (CST #3999, dilution 1:4000) was added to the membrane in 5% BSA TBST for 1 h at room temperature. Following three wash steps, Clarity Western ECL (BioRad) was added for 5 min prior to exposure of the membrane to film.

Mesotrypsin activity assay

Proteolytic activity of mesotrypsin and mesotrypsin labeled with the ABPP probe were determined as previously described (85). Briefly, enzyme at a concentration of 4 μM was incubated with 2.5 fold excess of probe or DMSO vehicle control (final DMSO concentration 0.11%), for 1 h at 37 °C, in DMEM/F12 phenol red–free medium. The colorimetric peptide reporter substrate Z-GPR-pNA (Sigma) was prepared as a 40× stock solution in 100% DMSO. Using the Varian Cary-100 spectrophotometer, the assays were carried out at 37 °C. Assay buffer (760 μl; 100 mM Tris–HCl pH 8.0, 1 mM $CaCl_2$) and substrate (20 μl) were mixed and equilibrated in cuvettes prior to reaction initiation. Enzyme + probe (20 μl) or enzyme + DMSO (20 μl) were added to start the reaction. The final reaction concentrations were as follows: enzyme at 0.5 nM, probe at 1.25 nM, and substrate at 100 μM. Reactions were followed for 5 min, and rates were determined from the absorbance increase upon the release of p-nitroaniline (ε410 = 8480 M^{-1} cm^{-1}).

Intact mass analysis with LC-MS using high resolution mass spectrometry

Mesotrypsin and catalytic mutant mesotrypsin-S195A at a concentration of 4 μM were incubated with 17 μM probe or DMSO control (final DMSO concentration 0.11%) for 1 h at 37 °C, in DMEM/F12 phenol red–free media at a final volume of 100 μl. LC-MS using a Thermo Scientific Orbitrap Elite Hybrid Mass Spectrometer (Thermo Fisher Scientific) coupled to a Thermo Ultimate 3000 RSLC HPLC system running a ProSwift RP-4H capillary monolithic column were used for capturing of data. The Elite was set to scan 500 to 3000 m/z at a resolution setting of 120,000 at 400 m/z. The spectra were deisotoped to give the intact MH+ mass using the Xtract function in Xcalibur.

Identification of the probe-labeled mesotrypsin peptide by nano-LC/MS using multiple fragmentation methods

Mesotrypsin (concentration 4 μM) was incubated with the probe (10 μM) for 1 h at 37 °C, and then samples were resolved by SDS-PAGE under denaturing conditions. The gel bands were destained and the gel pieces were dehydrated in acetonitrile, followed by reduction with rehydration in 50 mM tris(2-carboxyethyl)phosphine for 45 min at 60 °C. The reduced samples were then dehydrated in acetronitrile followed by rehydration in 25 mM iodoacetamide for alkylation at room temp for 45 min, followed by dehydration with acetonitrile. The proteins were digested using 0.25 μg trypsin (Promega) in 50 μl 25 mM Tris pH 8.2 and 0.0002% Zwitt 3-16 and incubated for 20 h at 37 °C. The digest solution was then subjected to TEV protease cleavage by adding 50 μl of TEV protease solution (0.0666 U/μl in 1× TEV buffer, Thermo) for 3 h at 37 °C. The extracted peptides were analyzed by nano-flow liquid chromatography electrospray tandem mass spectrometry using a Thermo Scientific Orbitrap Elite Hybrid Mass Spectrometer (Thermo Fisher Scientific) coupled to a Thermo Ultimate 3000 RSLCnano HPLC system with a

100 μm × 25 cm PicoFrit column packed with Agilent Poroshell EC C18 solid phase. The Elite mass spectrometer experiment was set to perform a FT full scan from 600 to 1600 m/z with resolution set at 120,000 (at 400 m/z), followed by orbitrap HCD MS/MS or ETD MS/MS scans on the top five ions set up for product ion–triggered data dependent MS3 on the neutral loss of the probe mass of 640.2966. The FTMS AGC target was set to 3e6 and the orbitrap MSn target was set to 4e5 with a max ion inject times of 100 ms for both. Dynamic exclusion was set to one and selected ions were placed on an exclusion list for 30 s. The raw files were analyzed using PEAKS software (Release Version 10) allowing for probe mass addition of 621.28 at serines, oxidation of methionine, and carbamidomethyl cysteine as variable modifications. A manually assembled small database of 118 human serine proteases which included human mesotrypsin and mesotrypsin-S195A mutant was searched to find probe-modified peptides, which were then manually validated. Search parameters used semi-specific trypsin specificity allowing for two missed cleavages with the precursor mass tolerance of 10 ppm and fragment tolerance of 0.02 Da. The protein identification criteria required a two peptide minimum and a false discovery rate (FDR) less than 1%. PEAKS estimates FDR using a decoy-fusion approach where a corresponding decoy sequence is appended to each sequence in the database. The matched probe-labeled mesotrypsin peptides gave peptide confidence scores (-10lgp) that were higher than the confidence scores removed when 1% FDR filter was applied.

HCD fragmentation led to the discovery of 11 b-type ions showing the probe attached to the peptide (Fig. S3), however, the most intense fragment detected was at 640.30D, which represents the probe by itself as it is removed from the peptide due to the fragmentation method. Using the more gentle ETD fragmentation approach, we identified a total of 19 c-type ions and no high intensity fragment at the size of the probe as detected before (Fig. S4).

Cell culture and reagents

JHOC5 and JHOC9 cells were purchased from RIKEN BioResource Research Center and cultured following supplier protocols in DMEM/F12 media with 1% NEAA (Gibco, Invitrogen) and JHOC5 cells with 10% fetal bovine serum and JHOC9 cells with 20% fetal bovine serum (Gemini Bio-Products), at 37 °C and humidified atmosphere with 5% CO_2.

Diminazene aceturate was purchased from Cayman Chemical Company (cat. #18678), gabexate mesylate from Sigma (SML2964-5MG), and hydroxystilbamidine CID 16212515, from NCI-DTP.

ABPP in-situ *labeling and purification*

Cell labeling

Cells were plated in the morning in complete media to allow attachment during the day; seeding was optimized to reach near confluency within 24 h. To collect sufficient secreted protein, cells were seeded into three 10 cm plates per condition. In the evening of the day of seeding, cells were washed 3× with 4 ml PBS followed by addition of 10 ml serum-free, phenol red–free media. The following morning, the PBS washes were repeated and finally 3 ml of serum-free, phenol red–free media was added for 24 h, to generate the conditioned media and accumulate secreted proteins.

The probe was resuspended in DMSO (stock solution 17 mM). All experimental procedures involving the probe were exclusively handled in LoBind protein tubes (Eppendorf). The probe was added directly to cell cultures in conditioned media to achieve final probe concentration of 5 μM and mixed by pipetting. DMSO was used as a vehicle control. The cells were returned to the incubator for 1 h at 37 °C. Following incubation, the conditioned medium was collected and spun 5 min at 1000 rpm at 4 °C to separate cell debris. The supernatant was removed and pooled from the three 10 cm plates; final volume of conditioned medium was 9 ml per test condition. Protease inhibitor (9 μl of 1000× stock Sigma p8340) and EDTA (final concentration 1 mM) were added to the supernatant. The conditioned medium was then concentrated using a 3K MWCO concentrator (Amicon, Millipore) to a final volume of 100 μl.

Precipitation

The concentrated conditioned media were mixed with four parts methanol, one part chloroform, and three parts water to precipitate proteins. Samples were briefly centrifuged and the upper aqueous layer was carefully removed and discarded, leaving the protein at the phase interface. An additional four parts of methanol was added and mixed, followed by high speed centrifugation for 5 min. Supernatant was carefully removed and the remaining protein pellet was briefly air dried.

Resolubilization and binding to beads

The protein pellet was solubilized in 100 μl 2.5% SDS PBS and heated for 5 min at 60 °C, followed by centrifugation at 6500*g* at room temperature to pellet residual insoluble protein. If a sizeable pellet remained, solubilization was repeated with an additional 50 μl 2.5% SDS PBS and incubation at 90 °C. Supernatants were combined and PBS was added to reach a final SDS concentration of 0.2%. Magnetic streptavidin beads (100 μl; Thermo Fisher, Pierce, #88816) were prepared as per manufacturer's instruction. Storage supernatant was removed from the beads and the protein solution in 0.2% SDS PBS was added to the beads and incubated under rotation for 3 h at room temperature to allow streptavidin–biotin interaction. Following a brief spin to remove beads trapped in the lid, the tubes were placed on magnetic stands and washed 1× with 0.2% SDS PBS, 5× with 1 ml PBS, and 5× with 1 ml of H_2O. Samples were then stored at 4 °C until further processing. Samples were used for mass spectrometry directly or, alternatively, were resolved by SDS-PAGE and then individual bands excised for MS protein identification (86).

qRT-PCR

Cellular RNA was isolated following the manufacturer's protocol, using TRIzol reagent (Invitrogen). RNA concentration

was determined by absorbance at 260/280 using the Nanodrop One spectrophotometer. Reverse transcribed cDNA was synthesized using the High Capacity cDNA Reverse Transcription Kit (Applied Biosystems). Reverse transcribed cDNA samples were analyzed using quantitative real-time PCR according to the manufacturer's protocol on the ABI QuantStudio 7 Flex Real-Time PCR System. Taqman assays for *PLAT* (Hs00263492), *PLAU* (Hs00170182), *PRSS1* (Hs00605631_g1), *PRSS2* (Hs00828418_gH), *PRSS3* (Hs00605637), *KLK6* (Hs00160519_m1), *ACTB* (Hs01060665_g1), and *GAPDH* (Hs99999905_m1) were obtained from Applied Biosystems and run over 40 cycles. Data were analyzed using QuantStudio Real-Time PCR Software (Applied Biosystems).

Lentiviral transduction

Lentiviral shRNA against *PLAT* and *PLAU* were obtained from the MISSION TRC1 and 1.5 libraries (Sigma). Knockdown efficiency of each gene was tested using five different constructs, and the two with the highest efficiency were selected for further experiments. Selected constructs targeting *PLAT* included NM_000930.2-1864c1c1 (KD1) and NM_000930.2-946s1c1 (KD2) and for *PLAU* included TRC1 NM_002658.1-1235s1c1 (KD1) and NM_002658.1-125s1c1 (KD2). For *KLK6*, KD1: NM_002774.2-297s1c1 and KD2: NM_002774.2-590s1c1. All experiments included control cultures transduced with nontarget shRNA control constructs not recognizing any human genes. Virus for transduction was produced using HEK 293FT cells following supplier protocols. For *PLAU*, *PLAT*, and *KLK6* KD using viral transduction, 8×10^5 cells of JHOC5 or JHOC9 were plated in 10 cm culture dishes to adhere overnight. Culture media were replaced with a mixture of 2.4 ml lentivirus-containing conditioned media, 3.5 μg/ml polybrene (EMD MILLIPORE Merck KGaA) and 3.6 ml complete culture media. After a 24 h incubation period, the supernatant was removed and replaced with complete media and 2 μg/ml (JHOC9) or 1 μg/ml (JHOC5) puromycin (Corning) for selection.

Invasion assay

JHOC5 and JHOC9 cells were transduced with *PLAT*, *PLAU*, or *KLK6* lentiviral shRNA constructs prior to the invasion assay. Cells were split 1:1.5 the day before the assay. On the day of the assay, BD BioCoat Matrigel Invasion Chambers (cat # 354480) were coated with 0.5 μg per well of Corning Matrigel Basement Membrane Matrix (cat # 354234) in serum-free DMEM/F12 media (cat # 10565-018 (Gibco)) and placed to polymerize for 4 to 5 h at 37 °C and 5% CO_2. Cells were trypsinized and pelleted before resuspension in 1 ml of 0.1% BSA/serum free DMEM/F12 media and counted using a Countess automated cell counter (Invitrogen). NIH/3T3 cell–conditioned serum-free medium (750 μl; DMEM supplemented with 50 μg/ml ascorbic acid) was used as chemoattractant. Cells were seeded in four replicates on top of the insert at a density of 5×10^4 (JHOC5) or 1.5×10^5 (JHOC9) cells (1×10^5 JHOC9 cell were used for the KLK6 invasion assay) in 500 μl final volume. For inhibitor treatment studies, 1.5×10^5 WT JHOC9 or 1×10^5 JHOC5 cells were seeded in the presence of 0, 1 μM, 10 μM, or 100 μM diminazene, 100 μM or 500 μM gabexate mesylate, or 10 μM or 100 μM hydroxystilbamidine (dissolved in DMSO; final DMSO concentration 1%) in 500 μl final volume. Cells were allowed to invade for 18 h (24 h for the diminazene and KLK6 experiments) at 37 °C in 5% CO_2. At the end of the assay, noninvading cells were removed from the insert by scrubbing with a cotton swab, and cells on the lower surface of the filter were fixed in 100% methanol for 30 min at −20 °C, followed by 1 h room temperature staining with 0.1% crystal violet in 20 mM MES, pH 6.0. Stained filters were photographed at 2× magnification and cells were counted using Image-Pro 7.0 or Infinity Analyze software.

Proliferation assay

Plate reader–based proliferation assays were performed on cells previously transduced with *PLAT*, *PLAU*, or *KLK6* KD virus. The cells were under selection for 5 days after virus addition prior to setting up the experiment. The day before the assay, 5000 cells/well in 100 μl complete media were plated into 96 well plates and incubated for 18 h. For diminazene, gabexate mesylate, and hydroxystilbamidine treatment experiments, cells were seeded at 5000 cells/well and incubated with vehicle only (DMSO at final concentration of 1%) or with each drug at the indicated final concentrations for 18 h in complete media before commencement of the assay. The assay was carried out following the manufacture's protocol (Promega CellTiter Glo 2.0 viability assay). Cells were lysed and incubated with Promega reagent and luminescent signal was acquired following the provided standard Promega protocol (Veritas, Turner BioSystems). Data were analyzed using GraphPad Prism 8.0.

Western blot analysis for tPA and uPA

JHOC9 cells transduced with *PLAU*-targeted or nontarget control lentiviral shRNA, or JHOC5 cells transduced with *PLAT*-targeted or nontarget control lentiviral shRNA, were seeded and cultured in 10 cm plates as detailed above for ABPP *in-situ* labeling. After 24 h in 3 ml of serum-free phenol red–free media at near confluency, cultures were labeled with 5 μM activity-based probe at 37 °C for 1 h as described. Supernatant was clarified and cell debris removed. Samples were then evaluated by Western blot for uPA (GeneTex GTX10046, dilution 1:1000; donkey anti-rabbit secondary GE Healthcare NA934V, dilution 1:3000) or tPA (Abcam #Ab227069, dilution 1:1000; donkey anti-rabbit secondary GE Healthcare NA934V, dilution 1:1000). Probe labeling was assessed using HRP-conjugated streptavidin (Cell Signaling #3999, incubation 1:7000, 1 h at RT). Membranes were washed three times and developed with Clarity Western ECL (BioRad) for 5 min before exposure to film.

Animal model, ascites collections, and Western blotting

Animal studies were conducted with approval by the Mayo Clinic Institutional Animal Care and Use Committee (IACUC) (protocol A00002844-17) according to protocols that we have

described in detail previously (51). Female Nod/SCID mice (6–8 weeks old) received an intraperitoneal injection with either JHOC9 (2×10^6) or JHOC5 (5×10^5) tumor cells injected into the lower right quadrant of the abdomen. JHOC9 cohorts were euthanized by CO_2 asphyxiation at 15 weeks and JHOC5 cohorts at 7 weeks due to tumor growth kinetics and moribund endpoints. Ascitic fluid was retrieved from the abdominal cavity and centrifuged to pellet the cellular component. The supernatant was collected and stored at −20 °C until use. Clarified supernatant (100 µl) was incubated with 16 µM activity-based probe for 1 h at 37 °C to achieve protein labeling. Samples were then evaluated by Western blot for uPA (Invitrogen MON-U-16-02, dilution 1:1000; goat anti-mouse secondary Thermo Scientific #31432, dilution 1:1000) or tPA (Abcam #Ab227069, dilution 1:1000; donkey anti rabbit secondary GE Healthcare NA934V, dilution 1:1000). Evidence of probe labeling was assessed using HRP-conjugated streptavidin (Cell Signaling #3999, incubation 1:7000, 1 h at RT). Membranes were washed three times and developed with Clarity Western ECL (BioRad) for 5 min before exposure to film.

Data availability

MS data have been deposited with MassIVE (ftp://MSV000087385@massive.ucsd.edu).

Supporting information—This article contains supporting information (88–90).

Acknowledgments—We would like to thank the Mayo Clinic Medical Genome Facility Proteomics Core for support and guidance in the development of the protocol. The Mayo Clinic Medical Genome Facility Proteomics Core is a shared resource of the Mayo Clinic Cancer Center (NCI P30 CA15083).

Author contributions—C. M., D. C. R., and E. S. R. conceptualization; C. M., B. M., R. E., and E. S. R. methodology; C. M., A. H., M. C., and B. M. investigation; C. M., A. H., M. C., and B. M. formal analysis; C. M. and B. M. data curation; C. M., A. H., M. C., and E. S. R. validation; C. M. and E. S. R. project administration; C. M., M. C., and E. S. R. visualization; C. M. and E. S. R. writing–original draft; C. M., A. H., M. C., B. M., R. E., D. C. R., and E. S. R. writing–review and editing; B. M., R. E., and E. S. R. resources; E. S. R. supervision; E. S. R. funding acquisition.

Funding and additional information—This work was supported by National Institutes of Health grants R21 CA226302, R01 CA154387, and R01 GM144393 to E. S. R. C. M. acknowledges support from the Mayo Clinic Graduate School of Biomedical Sciences. The content is solely the responsibility of the authors and does not necessarily represent the official views of the National Institutes of Health.

Conflict of interest—The authors declare that they have no conflicts of interest with the contents of this article.

Abbreviations—The abbreviations used are: ABPP, activity-based protein profiling; BSA, bovine serum albumin; DMF, dimethylformamide; DMSO, dimethyl sulfoxide; ETD, electron transfer dissociation; FDR, false discovery rate; Fmoc, fluorenylmethyloxycarbonyl; HCD, higher-energy collisional dissociation; KLK6, kallikrein 6; OCCC, Ovarian clear cell carcinoma; tBu, tert-butyl; TEV, tobacco etch virus; tPA, tissue plasminogen activator; uPA, urokinase-type plasminogen activator; uPAR, urokinase plasminogen activator receptor.

References

1. Groen, R. S., Gershenson, D. M., and Fader, A. N. (2015) Updates and emerging therapies for rare epithelial ovarian cancers: one size no longer fits all. *Gynecol. Oncol.* **136**, 373–383
2. Lheureux, S., Gourley, C., Vergote, I., and Oza, A. M. (2019) Epithelial ovarian cancer. *Lancet* **393**, 1240–1253
3. Gadducci, A., Multinu, F., Cosio, S., Carinelli, S., Ghioni, M., and Aletti, G. D. (2021) Clear cell carcinoma of the ovary: epidemiology, pathological and biological features, treatment options and clinical outcomes. *Gynecol. Oncol.* **162**, 741–750
4. Rawlings, N. D., Barrett, A. J., Thomas, P. D., Huang, X., Bateman, A., and Finn, R. D. (2017) The MEROPS database of proteolytic enzymes, their substrates and inhibitors in 2017 and a comparison with peptidases in the PANTHER database. *Nucleic Acids Res.* **46**, D624–D632
5. Mason, S. D., and Joyce, J. A. (2011) Proteolytic networks in cancer. *Trends Cell Biol.* **21**, 228–237
6. Di Cera, E. (2009) Serine proteases. *IUBMB Life* **61**, 510–515
7. Hedstrom, L. (2002) Serine protease mechanism and specificity. *Chem. Rev.* **102**, 4501–4524
8. Srinivasan, S., Kryza, T., Batra, J., and Clements, J. (2022) Remodelling of the tumour microenvironment by the kallikrein-related peptidases. *Nat. Rev. Cancer* **22**, 223–238
9. Martin, C. E., and List, K. (2019) Cell surface-anchored serine proteases in cancer progression and metastasis. *Cancer Metastasis Rev.* **38**, 357–387
10. Deu, E., Verdoes, M., and Bogyo, M. (2012) New approaches for dissecting protease functions to improve probe development and drug discovery. *Nat. Struct. Mol. Biol.* **19**, 9–16
11. Fortelny, N., Cox, J. H., Kappelhoff, R., Starr, A. E., Lange, P. F., Pavlidis, P., *et al.* (2014) Network analyses reveal pervasive functional regulation between proteases in the human protease web. *PLoS Biol.* **12**, e1001869
12. Sadaghiani, A. M., Verhelst, S. H., and Bogyo, M. (2007) Tagging and detection strategies for activity-based proteomics. *Curr. Opin. Chem. Biol.* **11**, 20–28
13. Nomura, D. K., Dix, M. M., and Cravatt, B. F. (2010) Activity-based protein profiling for biochemical pathway discovery in cancer. *Nat. Rev. Cancer* **10**, 630–638
14. Patricelli, M. P., Giang, D. K., Stamp, L. M., and Burbaum, J. J. (2001) Direct visualization of serine hydrolase activities in complex proteomes using fluorescent active site-directed probes. *Proteomics* **1**, 1067–1071
15. Sanman, L. E., and Bogyo, M. (2014) Activity-based profiling of proteases. *Annu. Rev. Biochem.* **83**, 249–273
16. Oleksyszyn, J., and Powers, J. C. (1991) Irreversible inhibition of serine proteases by peptide derivatives of (alpha-aminoalkyl)phosphonate diphenyl esters. *Biochemistry* **30**, 485–493
17. Abuelyaman, A. S., Hudig, D., Woodard, S. L., and Powers, J. C. (1994) Fluorescent derivatives of diphenyl [1-(N-peptidylamino)alkyl]phosphonate esters: synthesis and use in the inhibition and cellular localization of serine proteases. *Bioconjug. Chem.* **5**, 400–405
18. Jackson, D. S., Fraser, S. A., Ni, L.-M., Kam, C.-M., Winkler, U., Johnson, D. A., *et al.* (1998) Synthesis and evaluation of diphenyl phosphonate esters as inhibitors of the trypsin-like granzymes A and K and mast cell tryptase. *J. Med. Chem.* **41**, 2289–2301
19. Pan, Z., Jeffery, D. A., Chehade, K., Beltman, J., Clark, J. M., Grothaus, P., *et al.* (2006) Development of activity-based probes for trypsin-family serine proteases. *Bioorg. Med. Chem. Lett.* **16**, 2882–2885
20. Kam, C. M., Abuelyaman, A. S., Li, Z., Hudig, D., and Powers, J. C. (1993) Biotinylated isocoumarins, new inhibitors and reagents for detection, localization, and isolation of serine proteases. *Bioconjug. Chem.* **4**, 560–567

21. Haedke, U., Gotz, M., Baer, P., and Verhelst, S. H. (2012) Alkyne derivatives of isocoumarins as clickable activity-based probes for serine proteases. *Bioorg. Med. Chem.* **20**, 633–640
22. Haedke, U. R., Frommel, S. C., Hansen, F., Hahne, H., Kuster, B., Bogyo, M., *et al.* (2014) Phosphoramidates as novel activity-based probes for serine proteases. *ChemBioChem* **15**, 1106–1110
23. Joossens, J., Van der Veken, P., Surpateanu, G., Lambeir, A. M., El-Sayed, I., Ali, O. M., *et al.* (2006) Diphenyl phosphonate inhibitors for the urokinase-type plasminogen activator: optimization of the P4 position. *J. Med. Chem.* **49**, 5785–5793
24. Kasperkiewicz, P., Poreba, M., Snipas, S. J., Lin, S. J., Kirchhofer, D., Salvesen, G. S., *et al.* (2015) Design of a selective substrate and activity based probe for human neutrophil serine protease 4. *PLoS One* **10**, e0132818
25. Hawthorne, S., Hamilton, R., Walker, B. J., and Walker, B. (2004) Utilization of biotinylated diphenyl phosphonates for disclosure of serine proteases. *Anal. Biochem.* **326**, 273–275
26. Edgington-Mitchell, L. E., Barlow, N., Aurelio, L., Samha, A., Szabo, M., Graham, B., *et al.* (2017) Fluorescent diphenylphosphonate-based probes for detection of serine protease activity during inflammation. *Bioorg. Med. Chem. Lett.* **27**, 254–260
27. Speers, A. E., and Cravatt, B. F. (2005) A tandem orthogonal proteolysis strategy for high-content chemical proteomics. *J. Am. Chem. Soc.* **127**, 10018–10019
28. Weerapana, E., Speers, A. E., and Cravatt, B. F. (2007) Tandem orthogonal proteolysis-activity-based protein profiling (TOP-ABPP)–a general method for mapping sites of probe modification in proteomes. *Nat. Protoc.* **2**, 1414–1425
29. Morty, R. E., Troeberg, L., Pike, R. N., Jones, R., Nickel, P., Lonsdale-Eccles, J. D., *et al.* (1998) A trypanosome oligopeptidase as a target for the trypanocidal agents pentamidine, diminazene and suramin. *FEBS Lett.* **433**, 251–256
30. Perilo, C. S., Pereira, M. T., Santoro, M. M., and Nagem, R. A. P. (2010) Structural binding evidence of the trypanocidal drugs Berenil® and Pentacarinate® active principles to a serine protease model. *Int. J. Biol. Macromol.* **46**, 502–511
31. Kayode, O., Huang, Z., Soares, A. S., Caulfield, T. R., Dong, Z., Bode, A. M., *et al.* (2017) Small molecule inhibitors of mesotrypsin from a structure-based docking screen. *PLoS One* **12**, e0176694
32. Kulemina, L. V., and Ostrov, D. A. (2011) Prediction of off-target effects on angiotensin-converting enzyme 2. *J. Biomol. Screen.* **16**, 878–885
33. Menegatti, E., Bolognesi, M., Scalia, S., Bortolotti, F., Guarneri, M., and Ascenzi, P. (1986) Gabexate mesylate inhibition of serine proteases: thermodynamic and computer-graphics analysis. *J. Pharm. Sci.* **75**, 1171–1174
34. Stenman, U. H. (1990) Tumour-associated trypsin inhibitor and tumour-associated trypsin. *Scand. J. Clin. Lab. Invest. Suppl.* **201**, 93–101
35. Koivunen, E., Huhtala, M. L., and Stenman, U. H. (1989) Human ovarian tumor-associated trypsin. Its purification and characterization from mucinous cyst fluid and identification as an activator of pro-urokinase. *J. Biol. Chem.* **264**, 14095–14099
36. Ma, R., Ye, X., Cheng, H., Ma, Y., Cui, H., and Chang, X. (2015) PRSS3 expression is associated with tumor progression and poor prognosis in epithelial ovarian cancer. *Gynecol. Oncol.* **137**, 546–552
37. Thompson, R. C., and Blout, E. R. (1973) Restrictions on the binding of proline-containing peptides to elastase. *Biochemistry* **12**, 51–57
38. Bauer, C., Thompson, R., and Blout, E. (1976) The active centers of Streptomyces griseus protease 3 and α-chymotrypsin: enzyme-substrate interactions remote from the scissile bond. *Biochemistry* **15**, 1291–1295
39. Gosalia, D. N., Salisbury, C. M., Maly, D. J., Ellman, J. A., and Diamond, S. L. (2005) Profiling serine protease substrate specificity with solution phase fluorogenic peptide microarrays. *Proteomics* **5**, 1292–1298
40. Matsumura, M., Bhatt, A. S., Andress, D., Clegg, N., Takayama, T. K., Craik, C. S., *et al.* (2005) Substrates of the prostate-specific serine protease prostase/KLK4 defined by positional-scanning peptide libraries. *Prostate* **62**, 1–13
41. Harris, J. L., Niles, A., Burdick, K., Maffitt, M., Backes, B. J., Ellman, J. A., *et al.* (2001) Definition of the extended substrate specificity determinants for beta-tryptases I and II. *J. Biol. Chem.* **276**, 34941–34947
42. Barre, O., Dufour, A., Eckhard, U., Kappelhoff, R., Beliveau, F., Leduc, R., *et al.* (2014) Cleavage specificity analysis of six type II transmembrane serine proteases (TTSPs) using PICS with proteome-derived peptide libraries. *PLoS One* **9**, e105984
43. Takeuchi, T., Harris, J. L., Huang, W., Yan, K. W., Coughlin, S. R., and Craik, C. S. (2000) Cellular localization of membrane-type serine protease 1 and identification of protease-activated receptor-2 and single-chain urokinase-type plasminogen activator as substrates. *J. Biol. Chem.* **275**, 26333–26342
44. Herter, S., Piper, D. E., Aaron, W., Gabriele, T., Cutler, G., Cao, P., *et al.* (2005) Hepatocyte growth factor is a preferred *in vitro* substrate for human hepsin, a membrane-anchored serine protease implicated in prostate and ovarian cancers. *Biochem. J.* **390**, 125–136
45. Oleksyszyn, J., Boduszek, B., Kam, C.-M., and Powers, J. C. (1994) Novel amidine-containing peptidyl phosphonates as irreversible inhibitors for blood coagulation and related serine proteases. *J. Med. Chem.* **37**, 226–231
46. Bertrand, J. A., Oleksyszyn, J., Kam, C. M., Boduszek, B., Presnell, S., Plaskon, R. R., *et al.* (1996) Inhibition of trypsin and thrombin by amino(4-amidinophenyl)methanephosphonate diphenyl ester derivatives: X-ray structures and molecular models. *Biochemistry* **35**, 3147–3155
47. Szabo, R., and Bugge, T. H. (2008) Type II transmembrane serine proteases in development and disease. *Int. J. Biochem. Cell Biol.* **40**, 1297–1316
48. Andreasen, P. A., Kjøller, L., Christensen, L., and Duffy, M. J. (1997) The urokinase-type plasminogen activator system in cancer metastasis: a review. *Int. J. Cancer* **72**, 1–22
49. Dass, K., Ahmad, A., Azmi, A. S., Sarkar, S. H., and Sarkar, F. H. (2008) Evolving role of uPA/uPAR system in human cancers. *Cancer Treat. Rev.* **34**, 122–136
50. Petersen, L. C., Lund, L. R., Nielsen, L. S., Danø, K., and Skriver, L. (1988) One-chain urokinase-type plasminogen activator from human sarcoma cells is a proenzyme with little or no intrinsic activity. *J. Biol. Chem.* **263**, 11189–11195
51. Mehner, C., Miller, E., Hockla, A., Coban, M., Weroha, S. J., Radisky, D. C., *et al.* (2020) Targeting an autocrine IL-6-SPINK1 signaling axis to suppress metastatic spread in ovarian clear cell carcinoma. *Oncogene* **39**, 6606–6618
52. Boose, J. A., Kuismanen, E., Gerard, R., Sambrook, J., and Gething, M. J. (1989) The single-chain form of tissue-type plasminogen activator has catalytic activity: studies with a mutant enzyme that lacks the cleavage site. *Biochemistry* **28**, 635–643
53. Madison, E. L., Kobe, A., Gething, M. J., Sambrook, J. F., and Goldsmith, E. J. (1993) Converting tissue plasminogen activator to a zymogen: a regulatory triad of Asp-His-Ser. *Science* **262**, 419–421
54. Lawrence, M. S., Stojanov, P., Mermel, C. H., Robinson, J. T., Garraway, L. A., Golub, T. R., *et al.* (2014) Discovery and saturation analysis of cancer genes across 21 tumour types. *Nature* **505**, 495
55. Boycott, K. M., Vanstone, M. R., Bulman, D. E., and MacKenzie, A. E. (2013) Rare-disease genetics in the era of next-generation sequencing: discovery to translation. *Nat. Rev. Genet.* **14**, 681–691
56. Khan, A. R., and James, M. N. (1998) Molecular mechanisms for the conversion of zymogens to active proteolytic enzymes. *Protein Sci.* **7**, 815–836
57. Arolas, J. L., Goulas, T., Cuppari, A., and Gomis-Rüth, F. X. (2018) Multiple architectures and mechanisms of latency in metallopeptidase zymogens. *Chem. Rev.* **118**, 5581–5597
58. Lopez-Otin, C., and Hunter, T. (2010) The regulatory crosstalk between kinases and proteases in cancer. *Nat. Rev. Cancer* **10**, 278–292
59. Hauske, P., Ottmann, C., Meltzer, M., Ehrmann, M., and Kaiser, M. (2008) Allosteric regulation of proteases. *ChemBioChem* **9**, 2920–2928
60. Merdanovic, M., Monig, T., Ehrmann, M., and Kaiser, M. (2013) Diversity of allosteric regulation in proteases. *ACS Chem. Biol.* **8**, 19–26
61. Rawlings, N. D., Tolle, D. P., and Barrett, A. J. (2004) Evolutionary families of peptidase inhibitors. *Biochem. J.* **378**, 705–716
62. Otlewski, J., Jelen, F., Zakrzewska, M., and Oleksy, A. (2005) The many faces of protease-protein inhibitor interaction. *EMBO J.* **24**, 1303–1310

63. Liu, Y., Patricelli, M. P., and Cravatt, B. F. (1999) Activity-based protein profiling: the serine hydrolases. *Proc. Natl. Acad. Sci. U. S. A.* **96**, 14694–14699
64. Simon, G. M., and Cravatt, B. F. (2010) Activity-based proteomics of enzyme superfamilies: serine hydrolases as a case study. *J. Biol. Chem.* **285**, 11051–11055
65. Jessani, N., Humphrey, M., McDonald, W. H., Niessen, S., Masuda, K., Gangadharan, B., *et al.* (2004) Carcinoma and stromal enzyme activity profiles associated with breast tumor growth *in vivo*. *Proc. Natl. Acad. Sci. U. S. A.* **101**, 13756–13761
66. Nomura, D. K., Long, J. Z., Niessen, S., Hoover, H. S., Ng, S.-W., and Cravatt, B. F. (2010) Monoacylglycerol lipase regulates a fatty acid network that promotes cancer pathogenesis. *Cell* **140**, 49–61
67. Wang, C., Abegg, D., Dwyer, B. G., and Adibekian, A. (2019) Discovery and evaluation of new activity-based probes for serine hydrolases. *ChemBioChem* **20**, 2212–2216
68. Carmeliet, P., Moons, L., Lijnen, R., Baes, M., Lemaitre, V., Tipping, P., *et al.* (1997) Urokinase-generated plasmin activates matrix metalloproteinases during aneurysm formation. *Nat. Genet.* **17**, 439–444
69. van Dam, P. A., Coelho, A., and Rolfo, C. (2017) Is there a role for urokinase-type plasminogen activator inhibitors as maintenance therapy in patients with ovarian cancer? *Eur. J. Surg. Oncol.* **43**, 252–257
70. Radisky, E. S., and Radisky, D. C. (2010) Matrix metalloproteinase-induced epithelial-mesenchymal transition in breast cancer. *J. Mammary Gland Biol. Neoplasia* **15**, 201–212
71. Schmalfeldt, B., Prechtel, D., Harting, K., Spathe, K., Rutke, S., Konik, E., *et al.* (2001) Increased expression of matrix metalloproteinases (MMP)-2, MMP-9, and the urokinase-type plasminogen activator is associated with progression from benign to advanced ovarian cancer. *Clin. Cancer Res.* **7**, 2396–2404
72. Fischer, K., Lutz, V., Wilhelm, O., Schmitt, M., Graeff, H., Heiss, P., *et al.* (1998) Urokinase induces proliferation of human ovarian cancer cells: characterization of structural elements required for growth factor function. *FEBS Lett.* **438**, 101–105
73. Whitley, B. R., Palmieri, D., Twerdi, C. D., and Church, F. C. (2004) Expression of active plasminogen activator inhibitor-1 reduces cell migration and invasion in breast and gynecological cancer cells. *Exp. Cell Res.* **296**, 151–162
74. Kenny, H. A., Leonhardt, P., Ladanyi, A., Yamada, S. D., Montag, A., Im, H. K., *et al.* (2011) Targeting the urokinase plasminogen activator receptor inhibits ovarian cancer metastasis. *Clin. Cancer Res.* **17**, 459
75. Hapke, S., Kessler, H., de Prada, N. A., Benge, A., Schmitt, M., Lengyel, E., *et al.* (2001) Integrin αvβ3/vitronectin interaction affects expression of the urokinase system in human ovarian cancer cells. *J. Biol. Chem.* **276**, 26340–26348
76. Fugate, J. E., and Rabinstein, A. A. (2014) Update on intravenous recombinant tissue plasminogen activator for acute ischemic stroke. *Mayo Clin. Proc.* **89**, 960–972
77. Nagy, J. A., Meyers, M. S., Masse, E. M., Herzberg, K. T., and Dvorak, H. F. (1995) Pathogenesis of ascites tumor growth: fibrinogen influx and fibrin accumulation in tissues lining the peritoneal cavity. *Cancer Res.* **55**, 369–375
78. Wilhelm, O., Hafter, R., Coppenrath, E., Pflanz, M. A., Schmitt, M., Babic, R., *et al.* (1988) Fibrin-fibronectin compounds in human ovarian tumor ascites and their possible relation to the tumor stroma. *Cancer Res.* **48**, 3507–3514
79. Jandu, N., Richardson, M., Singh, G., Hirte, H., and Hatton, M. W. (2006) Human ovarian cancer ascites fluid contains a mixture of incompletely degraded soluble products of fibrin that collectively possess an anti-angiogenic property. *Int. J. Gynecol. Cancer* **16**, 1536–1544
80. Diaz, V. M., Planaguma, J., Thomson, T. M., Reventos, J., and Paciucci, R. (2002) Tissue plasminogen activator is required for the growth, invasion, and angiogenesis of pancreatic tumor cells. *Gastroenterology* **122**, 806–819
81. Hurtado, M., Lozano, J. J., Castellanos, E., Lopez-Fernandez, L. A., Harshman, K., Martinez, A. C., *et al.* (2007) Activation of the epidermal growth factor signalling pathway by tissue plasminogen activator in pancreas cancer cells. *Gut* **56**, 1266–1274
82. Paciucci, R., Tora, M., Diaz, V. M., and Real, F. X. (1998) The plasminogen activator system in pancreas cancer: role of t-PA in the invasive potential *in vitro*. *Oncogene* **16**, 625–633
83. Diaz, V. M., Hurtado, M., Thomson, T. M., Reventos, J., and Paciucci, R. (2004) Specific interaction of tissue-type plasminogen activator (t-PA) with annexin II on the membrane of pancreatic cancer cells activates plasminogen and promotes invasion *in vitro*. *Gut* **53**, 993–1000
84. Yamashita, D., Kondo, T., Ohue, S., Takahashi, H., Ishikawa, M., Matoba, R., *et al.* (2015) miR340 suppresses the stem-like cell function of glioma-initiating cells by targeting tissue plasminogen activator. *Cancer Res.* **75**, 1123–1133
85. Salameh, M. A., Soares, A. S., Hockla, A., and Radisky, E. S. (2008) Structural basis for accelerated cleavage of bovine pancreatic trypsin inhibitor (BPTI) by human mesotrypsin. *J. Biol. Chem.* **283**, 4115–4123
86. Steen, H., and Mann, M. (2004) The ABC's (and XYZ's) of peptide sequencing. *Nat. Rev. Mol. Cell Biol.* **5**, 699–711
87. Berger, A., and Schechter, I. (1967) On the size of the active site in proteases. I. Papain. *Biochem. Biophys. Res. Commun.* **27**, 157–162
88. Kojima, Y., Machida, Y., Palani, S., Caulfield, T. R., Radisky, E. S., Kaufmann, S. H., *et al.* (2020) FAM111A protects replication forks from protein obstacles via its trypsin-like domain. *Nat. Commun.* **11**, 1–14
89. Acharya, S., Dutta, S., and Bose, K. (2020) A distinct concerted mechanism of structural dynamism defines activity of human serine protease HtrA3. *Biochem. J.* **477**, 407–429
90. Kubo, H., Matsushita, M., Kotani, M., Kawasaki, H., Saido, T. C., Kawashima, S., *et al.* (1999) Molecular basis for oviductin-mediated processing from gp43 to gp41, the predominant glycoproteins of Xenopus egg envelopes. *Dev. Genet.* **25**, 123–129